

In vivo imaging of neuroprotection in stroke:
In search of the penumbra

Katy Marie Orchowski

Master of Science
Department of Neurology and Neurosurgery

McGill University
Montreal, Quebec, Canada

June 2012

A thesis submitted to McGill University in partial fulfillment of the
requirements of the degree of Master of Science

© Katy Marie Orchowski 2012

Dedication

This document is dedicated to my loving family for their ceaseless support of my endeavors, especially my pappy, Harry Orchowski, who truly appreciated the value of education.

Acknowledgements

To begin with, I would like to thank my family and friends for their infinite espousal of my education, particularly Chris, who selflessly encouraged me to pursue an advanced degree over 600 miles away from him. Also, I am tremendously grateful for the precious collaboration with the Université de Montréal, where Numa Dancause and Stephan Quessy generously provided their skills and expertise for the animal model used in this study. I would moreover like to recognize Alexey Kostikov, Miriam Kovacevic, and Dean Jolly for performing the radiotracer syntheses and providing guidance on chemistry-related matters, and Antonio Aliaga for managing the positron emission tomography scans. Additionally, I am grateful for the help of Peter Zepper and Basia Radlinska in learning how to analyze the raw positron emission tomography data. Furthermore, I very much appreciate the invaluable feedback provided by my advisory committee members, Esther Schirmacher and Jean-Paul Soucy, as well as my supervisors Ralf Schirmacher and Alexander Thiel. Thank both of you for shaping this project, providing support at each step along the way, and always keeping my best interests in mind.

Table of Contents

Dedication.....	ii
Acknowledgements.....	iii
Table of Contents.....	iv
List of Tables.....	vi
List of Figures.....	vii
Abstract.....	viii
Résumé.....	x
Chapter 1. Background.....	1
1.1 Introduction.....	1
1.1.1 Ischemic Stroke.....	1
1.1.2 The "Penumbra" Concept.....	3
1.1.3 Thrombolytic Therapy.....	4
1.1.4 Diagnostic Imaging Methods.....	5
1.1.5 Positron Emission Tomography.....	7
1.1.6 Imaging the Penumbra with Positron Emission Tomography.....	8
1.2 Current Study.....	9
1.2.1 Aim.....	9
1.2.2 Objectives.....	11
1.2.2.1 Radioactively Labeling Erythropoietin with Fluorine-18.....	11
1.2.2.2 Establishing a Penumbra in the Endothelin-1 Stroke Model....	11
1.2.2.3 Exploring [¹⁸ F]-Erythropoietin as a Penumbra Radiotracer....	12
Chapter 2. Radioactively Labeling Erythropoietin with Fluorine-18.....	13
2.1 Introduction.....	13
2.1.1 Erythropoietin.....	13
2.1.2 Fluorine-18.....	15
2.1.3 Predictions.....	16
2.2 Methods.....	16
2.2.1 Materials.....	16
2.2.2 Synthesis of [¹⁸ F]-SFB and [¹⁸ F]-Erythropoietin.....	17
2.2.3 Quality Control of [¹⁸ F]-Erythropoietin.....	18
2.3 Quality Control Results.....	18
2.4 Discussion.....	19
Chapter 3. Establishing a Penumbra in the Endothelin-1 Stroke Model.....	20
3.1 Introduction.....	20
3.1.1 Endothelin-1 Model of Focal Ischemia.....	20
3.1.2 ¹⁸ F-Fluoromisonidazole.....	21
3.1.3 Predictions.....	22
3.2 Methods.....	22
3.2.1 Materials.....	22
3.2.2 Synthesis of [¹⁵ O]-Water and [¹⁸ F]-FMISO.....	23

3.3.3 Animals.....	24
3.3.4 Surgery.....	24
3.3.5 Data Acquisition.....	25
3.3.6 Data Analysis.....	27
3.3 Results.....	28
3.3.1 Within-Group Comparisons.....	28
3.3.2 Between-Group Comparisons.....	31
3.3.3 Pooled Analysis of Cerebral Blood Flow Images.....	33
3.4 Discussion.....	33
Chapter 4. Exploring [18F]-Erythropoietin as a Penumbra Radiotracer.....	37
4.1 Introduction.....	37
4.1.1 <i>In Vivo</i> Properties of Erythropoietin.....	37
4.1.2 Predictions.....	38
4.2 Methods.....	38
4.2.1 Materials.....	38
4.2.2 Synthesis of [15O]-Water and [18F]-Erythropoietin.....	39
4.2.3 Animals.....	39
4.2.4 Surgery.....	40
4.2.5 Data Acquisition.....	40
4.2.6 Data Analysis.....	41
4.3 Results.....	47
4.3.1 Within-Group Comparisons.....	47
4.3.2 Between-Group Comparisons.....	50
4.4 Discussion.....	52
Chapter 5. General Discussion.....	54
5.1 Summary of Results.....	54
5.2 Limitations.....	55
5.3 Future Directions.....	55
5.4 Conclusions.....	56
List of References.....	58

List of Tables

Table 1. Locations of endothelin-1 injections.....	25
Table 2. [¹⁵ O]-Water descriptive statistics for Objective 2.....	29
Table 3. [¹⁸ F]-FMISO descriptive statistics.....	30
Table 4. Summary of paired t-tests for Objective 2.....	31
Table 5. Summary of unpaired t-tests for Objective 2.....	33
Table 6. Pooled [¹⁵ O]-Water standard uptake value ratio descriptive statistics.....	33
Table 7. [¹⁵ O]-Water descriptive statistics for Objective 3.....	43
Table 8. Descriptive statistics for [¹⁸ F]-Erythropoietin (frames 1-6).....	44
Table 9. Descriptive statistics for [¹⁸ F]-Erythropoietin (frames 7-12).....	45
Table 10. Descriptive statistics for [¹⁸ F]-Erythropoietin (frames 13-18).....	46
Table 11. Summary of paired t-tests for Objective 3.....	47
Table 12. Summary of unpaired t-tests for Objective 3.....	51
Table 13. Summary of between-group comparisons for standard uptake value ratios of [¹⁸ F]-FMISO and [¹⁸ F]-Erythropoietin.....	51

List of Figures

Figure 1: A blood clot resulting from plaque buildup in an artery leading to the brain.....	2
Figure 2: Positron emission tomography scans of a patient with ischemic stroke in the left middle cerebral artery.....	10
Figure 3: Chromatogram of [¹⁸ F]-Erythropoietin, illustrating the purified protein peak forming at fifteen minutes.....	19
Figure 4: Experimental time line for Objective 2.....	26
Figure 5: Positron emission tomography standard uptake value images of Objective 2 stroke group.....	28
Figure 6: Positron emission tomography standard uptake value images of Objective 2 control group.....	31
Figure 7: Average [¹⁵ O]-Water standard uptake values (\pm SD) for Objective 2, presented by experimental condition within both hemispheres.....	32
Figure 8: Average [¹⁸ F]-FMISO standard uptake values (\pm SD), presented by experimental condition within both hemispheres.....	32
Figure 9: Experimental time line for Objective 3.....	41
Figure 10: Positron emission tomography standard uptake value images of [¹⁸ F]-Erythropoietin in stroke group, shown in transaxial, coronal, and sagittal planes, respectively.....	48
Figure 11: Positron emission tomography standard uptake value images of [¹⁸ F]-Erythropoietin in control group, shown in transaxial, coronal, and sagittal planes, respectively.....	49
Figure 12: Average [¹⁵ O]-Water standard uptake values (\pm SD) for Objective 3, presented by experimental condition within both hemispheres.....	50

Figure 13: Average [¹⁸F]-Erythropoietin standard uptake values (\pm SD) at one, two, and three hours, presented by experimental condition within both hemispheres.....50

Figure 14: Transaxial, coronal, and sagittal sections of positron emission tomography standard uptake values for A) [¹⁸F]-FMISO, showing uptake in area of stroke, and B) [¹⁸F]-Erythropoietin, showing no uptake in the same area.....52

Abstract

When a stroke occurs, physicians can use positron emission tomography to determine the extent of brain damage; however, there is not currently a single positron emission tomography tracer that provides precise information regarding the size and location of the ischemic penumbra. As the erythropoietin receptor is selectively upregulated in the penumbra, radioactively labeled erythropoietin may provide more specific information about this area than current penumbra tracers. We hypothesize that the new positron emission tomography tracer [^{18}F]-Erythropoietin will reveal the penumbra better than established positron emission tomography tracers, thereby providing physicians with an alternative option for stroke diagnosis. To test this, we injected endothelin-1 in the motor cortex of rats to induce stroke. Within three hours of stroke onset, rats first received an intravenous injection of the cerebral blood flow tracer [^{15}O]-Water, followed by an injection of either [^{18}F]-Fluoromisonidazole, a possible penumbra tracer, or [^{18}F]-Erythropoietin, our experimental tracer. Then, the animals were scanned using positron emission tomography. In contrast to what was expected from immunohistological studies, we found that [^{18}F]-Erythropoietin did not bind to ischemic tissue in the brain to effectively distinguish the penumbra from the core of a stroke. In fact, [^{18}F]-Erythropoietin did not even enter the brain, at least not in sufficient amounts to be quantified with positron emission tomography. Taken together, our results demonstrate that [^{18}F]-Erythropoietin is not an effective penumbra tracer in our animal model. More work is needed to optimize the *in vivo* properties of [^{18}F]-Erythropoietin in order for it to be a valuable tracer for neuroimaging. Establishing a new penumbra tracer would enable physicians to easily determine whether living tissue exists in patients following an acute

ischemic stroke, thereby facilitating the decision to proceed with potentially beneficial therapies.

Résumé

Lors d'un accident vasculaire cérébral, les médecins peuvent utiliser la tomographie par émission de positrons pour déterminer l'étendue des dommages au cerveau. Maintenant, il n'y a pas de traceurs actuellement utilisés en tomographie par émission de positrons qui fournissent l'informations précises, comme la taille et la location de la pénombre ischémique. Puisque le récepteur de l'érythropoïétine est régulé à la hausse dans la pénombre, l'utilisation de l'érythropoïétine marquée radioactivement pourrait fournir des informations plus précises sur cette région que les traceurs de pénombre actuels. Nous avons donc émis l'hypothèse que le nouveau traceur [^{18}F]-Érythropoïétine révélera la pénombre mieux que les traceurs déjà établis, fournissant ainsi aux médecins une option alternative pour le diagnostic d'accident vasculaire cérébral. Pour tenter de vérifier cette hypothèse, nous avons injecté l'endothéline-1 dans le cortex moteur de rats pour induire un accident vasculaire cérébral. Dans les trois heures suivant l'apparition des symptômes, des rats ont reçu le traceur débit sanguin cérébral [^{15}O]-Eau, suivie par une injection intraveineuse soit de [^{18}F]-Fluoromisonidazole, un traceur de pénombre possible, ou de [^{18}F]-Érythropoïétine, notre traceur expérimental. Ensuite, les animaux ont été scannés à l'aide de la tomographie par émission de positrons. Contrairement à ce qui était attendu à partir d'études immunohistologiques, nous avons constaté que la [^{18}F]-Érythropoïétine ne s'est liée au tissu ischémique dans le cerveau pour distinguer efficacement la pénombre du coeur d'un accident vasculaire cérébral. En fait, la [^{18}F]-Érythropoïétine n'a même pas pénétré dans le cerveau, du moins pas en quantité suffisante pour être quantifiée avec la tomographie par émission de positrons. Pris dans leur ensemble, nos résultats démontrent que la [^{18}F]-Érythropoïétine n'est pas un traceur de

pénombre efficace dans notre modèle animal. Plus de travail est nécessaire pour optimiser les propriétés *in vivo* de la [¹⁸F]-Érythropoïétine afin qu'elle devienne un traceur utile et efficace pour la neuro-imagerie. L'objectif principal du développement d'un nouveau traceur de pénombre serait de permettre aux cliniciens de déterminer facilement si le tissu vivant existe chez les patients qui subissent un accident vasculaire cérébral ischémique aigu, ce qui faciliterait la prise de décision afin de procéder à des thérapies potentiellement bénéfiques.

- Chapter 1 -

Background

1.1 Introduction

A stroke occurs when blood flow to the brain is disrupted, preventing the delivery of vital oxygen to dependent brain cells. Of the roughly 795,000 annual cases, a small portion are due to hemorrhaging, while an overwhelming 87% are the result of ischemic attacks (Roger et al., 2012). Stroke symptoms widely vary depending on the areas of the brain that are affected, but common signs range from numbness to speech and motor impairment. If symptoms are recognized early, medical interventions are better able to prevent a stroke from damaging even more of the brain than it already does.

The present study investigates a potential new tool to identify the area of a stroke that can benefit from interventions. Both researchers and physicians are greatly in need of a simple method to identify this at-risk area, as current imaging methods are ambiguous and dauntingly time-consuming.

1.1.1 Ischemic Stroke

The most prevalent strokes are ischemic in nature. These occur when there is a sudden disruption of blood flow that precludes the delivery of oxygen and glucose to the brain, usually resulting from a blood clot or an embolus (Hinkle and Guanci, 2007). A major contributor to ischemic stroke

is plaque buildup within the blood vessels, which narrows the opening for blood to flow through the arteries leading to the brain. Once plaque forms, platelets adhere to it and rapidly build up; this aggregation eventually causes a clot to develop (Hinkle and Guanci, 2007), as illustrated in Figure 1. Alternately, an artery can be blocked by an embolus, such as fat, air, or blood clots, that originates from somewhere else in the body (Hinkle and Guanci, 2007). When blood flow is interrupted, the brain does not receive sufficient energy to properly function, as energy is derived from oxygen in the blood. Since the brain requires a great deal of energy to operate at a normal level, it is highly susceptible to ischemic damage. As blood and oxygen levels fall, the brain can no longer produce adenosine triphosphate, its most common source of energy. Without adequate blood flow, neurons quickly run out of energy reserves, lose function, and ultimately die if blood flow is not reinstated within a relatively brief period of time (Heiss, 2011). This hypoperfused, vulnerable area is known as the ischemic penumbra.

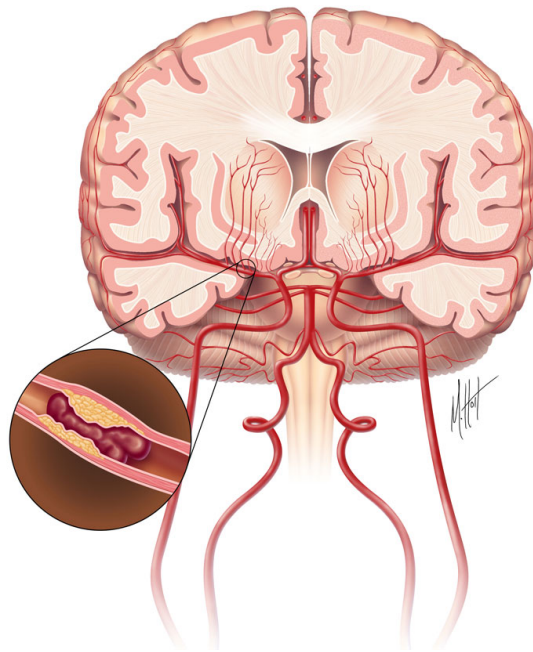


Figure 1 (from (Center, 2012).

A blood clot resulting from plaque buildup in an artery leading to the brain.

1.1.2 The "Penumbra" Concept

The immediate tissue that is affected by a stroke, labeled the core, becomes necrotic within a few hours. Surrounding the core is an ischemic, yet viable, area known as the penumbra, which is at high risk for evolving into necrotic tissue (Astrup et al., 1981). As time progresses, the core spreads into this initially salvageable tissue by means of apoptosis, neuroinflammation, and excitotoxicity (van der Kooij et al., 2008). To prevent the infarct from spreading, blood circulation must be reinstated as quickly as possible. Otherwise, these mechanisms of delayed cell death can be responsible for as much as 20% of the final infarct size (Heiss et al., 2004). In order to determine if medical intervention can prevent this process from occurring, it is necessary to establish whether penumbra tissue exists in a stroke patient.

Tissue viability after a stroke can be determined by cerebral blood flow. For instance, cerebral blood flow is typically 60-100 milliliters/100 grams·minute under normal conditions (Heiss, 2000). Within the brain, neuronal maintenance and transmission require different amounts of energy, thereby establishing two oxygen-dependent limits: the functional and viability thresholds (Heiss, 2011). Neurotransmission stops when cerebral blood flow reaches the functional threshold (20 milliliters/100 grams·minute), with cellular damage and death occurring if cerebral blood flow drops below the viability threshold (6-15 milliliters/100 grams·minute) (Heiss, 2000). If cerebral blood flow falls below the functional threshold, reperfusion enables neurons to regain function. However, if cerebral blood flow further slows, neurons eventually reach the time-dependent viability threshold, at which point vascular perfusion is too low for cells to survive (Heiss, 2000). In other words, neuronal fate depends on both the severity at which cerebral blood flow slows and the length of time that cells are exposed to toxic conditions

(Furlan et al., 1996). For example, if tissue perfusion falls below this threshold for a brief period, then regains perfusion, it may likely survive; however, if perfusion further decreases below the viability threshold and remains there, tissue quickly becomes necrotic. Thus, the lower the cerebral blood flow, the higher the risk of necrosis.

The core of a stroke becomes necrotic because cerebral blood flow drops below the viability threshold for too long. Within the penumbra, perfusion remains above the viability threshold because the tissue is supplied with blood from collateral arteries. However, this supply is not sufficient to maintain the energy demands of the ischemic region, which places the penumbra at very high risk for evolving into necrotic tissue. Although this region is functionally impaired, it is capable of surviving since cerebral blood flow is maintained between the viability and functional thresholds for somewhat extended periods of time (Heiss, 2000). There are conflicting reports regarding the exact threshold at which tissue becomes "at risk" in humans (Dani et al., 2011), and it is currently not possible to determine the amount of time that tissue is critically hypoperfused (Heiss, 2011). Consequently, physicians cannot reliably use these criteria to operationally define the penumbra. Still, these characteristics render the penumbra a unique area where metabolic activity continues for a period of time despite the stoppage of blood flow. Not so surprisingly, this time-dependent area of a stroke is the target for both approved and experimental therapeutics.

1.1.3 Thrombolytic Therapy

Presently, the only curative stroke intervention is the administration of thrombolytic drugs, such as recombinant tissue plasminogen activator, that restore blood flow to the affected area of the brain by trying to dissolve the blood clot (Suwanwela and Koroshetz, 2007). There is some risk for severe

bleeding to occur during the administration of recombinant tissue plasminogen activator, which is given intravenously over the course of an hour. In addition to continuous monitoring throughout the duration of this treatment, a patient undergoes a neurological assessment every fifteen minutes.

First approved by the Food and Drug Administration in 1996, intravenous recombinant tissue plasminogen activator must be administered within three hours of stroke onset, when current practice maintains that the ischemic penumbra still exists. Assuming that penumbral tissue is only present for up to three hours in all individuals is incorrect, as the existence of penumbra tissue is extremely variable across patients. In fact, some individuals have viable tissue in the penumbra for up to eight hours after stroke onset (Baron et al., 1995). Since some patients may still benefit from therapeutic interventions well after the strict three-hour time frame, it is necessary to develop a method that clearly determines the amount of penumbra tissue that can be saved.

1.1.4 Diagnostic Imaging Methods

When imaging stroke, physicians aim to determine: 1) the presence of a hemorrhage; 2) the presence of a blood clot; 3) the extent of irreversibly damaged tissue; and 4) possibly salvageable but hypoperfused at-risk tissue (Latchaw et al., 2009). These functional imaging parameters are vital to accurate stroke diagnosis and treatment; however, current imaging methods lack refinement, requiring a battery of tests in order to assess an individual's prognosis (Hinkle and Guanci, 2007). Depending on the amount of time between stroke onset and treatment, different imaging methods are employed. Typically, a computed tomography scan is first conducted to confirm the type of stroke and the affected area, although magnetic

resonance imaging can also determine whether a stroke is ischemic or hemorrhagic in nature (Muir et al., 2006). This information helps physicians determine how to appropriately proceed with treatment. Computed tomography or magnetic resonance angiography can be used to ascertain even more specific information about the cerebral vasculature (Muir et al., 2006), which can further facilitate treatment options. Another common practice combines either magnetic resonance imaging or computed tomography with positron emission tomography in order to localize metabolic activity to specific structures in the brain (Muir et al., 2006). Although this method undoubtedly provides the most information, it is also the most time consuming. Since time is the utmost factor in stroke treatment, it is somewhat impractical to obtain all of this information through this technique.

These different imaging modalities can moreover define the penumbra of a stroke. With magnetic resonance imaging, the penumbra is defined by mismatching scans of diffusion- and perfusion-weighted imaging (Muir et al., 2006). Diffusion-weighted imaging shows tissue integrity, while perfusion-weighted imaging reveals cerebral perfusion. Yet perfusion-weighted imaging does not directly measure cerebral blood flow; instead, it measures the time needed to the minimum perfusion signal, or time-to-peak. Additionally, this method does not reliably measure the oxygen extraction fraction, which is characteristically heightened in the penumbra, and it overestimates at-risk tissue compared to positron emission tomography (Sobesky et al., 2005). This is problematic because it mistakenly reveals more salvageable tissue than there actually exists.

Positron emission tomography is the gold standard in stroke imaging (Heiss, 2000). Still, multiple positron emission tomography parameters are

necessary in order to operationally define the penumbra (Baron, 2001). In fact, the foremost issue with all of these imaging methods is that a single test is not definitive in itself. A patient must undergo multiple tests in order to evaluate the ischemic penumbra. There is a need for a sounder way of identifying neuronal integrity within penumbra so that precious time and resources are saved, thereby allocating more time to treating a patient rather than submitting him or her to an array of tests.

1.1.5 Positron Emission Tomography

Positron emission tomography is a noninvasive neuroimaging technique that measures the distribution of radioactively labeled molecules, known as radiotracers, in a living organism. A radiotracer consists of a radioactive nuclide, such as carbon-11 or fluorine-18, attached to a biological molecule. When very small concentrations of a radiotracer are injected into a living organism, the biological distribution of these radioactively labeled molecules can be ascertained.

As a radionuclide decays, positrons are emitted. These travel away from the radionuclide, losing energy as they do so. Once a positron exhausts a certain maximal energy, it collides with an electron, its antiparticle. This collision results in an annihilation event that produces two 511 kilo-electron volt gamma rays traveling in directions approximately 180 degrees opposite to one another (Wahl and Buchanan, 2002). A positron emission tomography scanner detects pairs of gamma rays with a ring of scintillation detectors. These coincidence events are then grouped into signograms and reconstructed to form a three-dimensional image of the radiotracer's *in vivo* distribution (Wahl and Buchanan, 2002).

When selecting a radionuclide for positron emission tomography imaging, one must consider the maximal energy and half-life. Radionuclides

with lower maximal energy emit positrons that travel shorter distances from the parent isotope, thus producing images with better spatial resolution (Wahl and Buchanan, 2002). Additionally, a longer half-life allows for imaging to occur over a longer amount of time, which improves image quality and enables researchers to learn more about a radiotracer's biological distribution over time. Still, a longer half-life also increases a subject's exposure to radiation (Wahl and Buchanan, 2002).

Compared to other imaging techniques, positron emission tomography is not widely used because it requires either large cyclotrons to produce radionuclides or the timely delivery of radionuclides produced in other facilities. Still, its ability to directly measure cerebral blood flow makes positron emission tomography the gold standard in stroke imaging (Heiss, 2000), especially since it quantifies the amount of radioactivity in a target region of interest, as measured by standard uptake values. Positron emission tomography also directly images biochemical processes like neurotransmitter binding, a phenomenon that cannot be measured with other imaging modalities. Taken together, the absolute quantification of radioactivity and ability to image both biological and biochemical processes provide specific information about the quantity and location of a radiotracer's uptake at a given point in time, which is extremely beneficial to researchers and physicians alike.

1.1.6 Imaging the Penumbra with Positron Emission Tomography

When imaging a stroke with positron emission tomography, it is necessary to establish cerebral blood flow to determine the extent of damage caused by the infarct. The core can be easily ascertained, as there is no flow in this area of the infarct, where the blood-brain barrier is entirely compromised. One technique utilizes the radiotracer [¹⁵O]-Water, a common

marker of cerebral blood flow in humans (Ito et al., 2004). Alternatively, cerebral blood flow may be determined with single-photon emission computed tomography, computed tomography, and magnetic resonance (Taber et al., 2005), as well as various optical approaches (Wang et al., 2003).

In addition to establishing a map of cerebral blood flow, other parameters are necessary in order to obtain a rough approximation of the penumbra. Most commonly, cerebral blood flow images are superimposed with images of the cerebral metabolic rate of oxygen, a measure of cellular metabolism (Heiss, 2011). The penumbra is the area where there is little or no cerebral blood flow, but the cerebral metabolic rate of oxygen is preserved, as shown in Figure 2. Several radiotracers may reveal the penumbra, such as [¹⁸F]-Fluoromisonidazole ([¹⁸F]-FMISO), which produces a positive image of hypoxic, at-risk tissue in the brain. Nonetheless, this radiotracer is not completely validated as a reliable penumbra marker (Muir et al., 2006), as it does not differentiate tissue that is below the functional threshold from tissue that is beyond the viability threshold. There is a need for a radiotracer that specifically targets the penumbra, thereby simplifying the process of identifying this area with neuroimaging.

1.2 Current Study

1.2.1 Aim

This study aims to develop a novel radiotracer for positron emission tomography imaging that exclusively reveals the ischemic penumbra. To accomplish this, we must first successfully label a molecule of interest with a radionuclide. To this end, we chose the neuroprotective protein erythropoietin, as its receptor is selectively upregulated in the ischemic penumbra of a stroke (Siren et al., 2001). In order to effectively evaluate the *in vivo* properties of erythropoietin, we attempted to label it with fluorine-18,

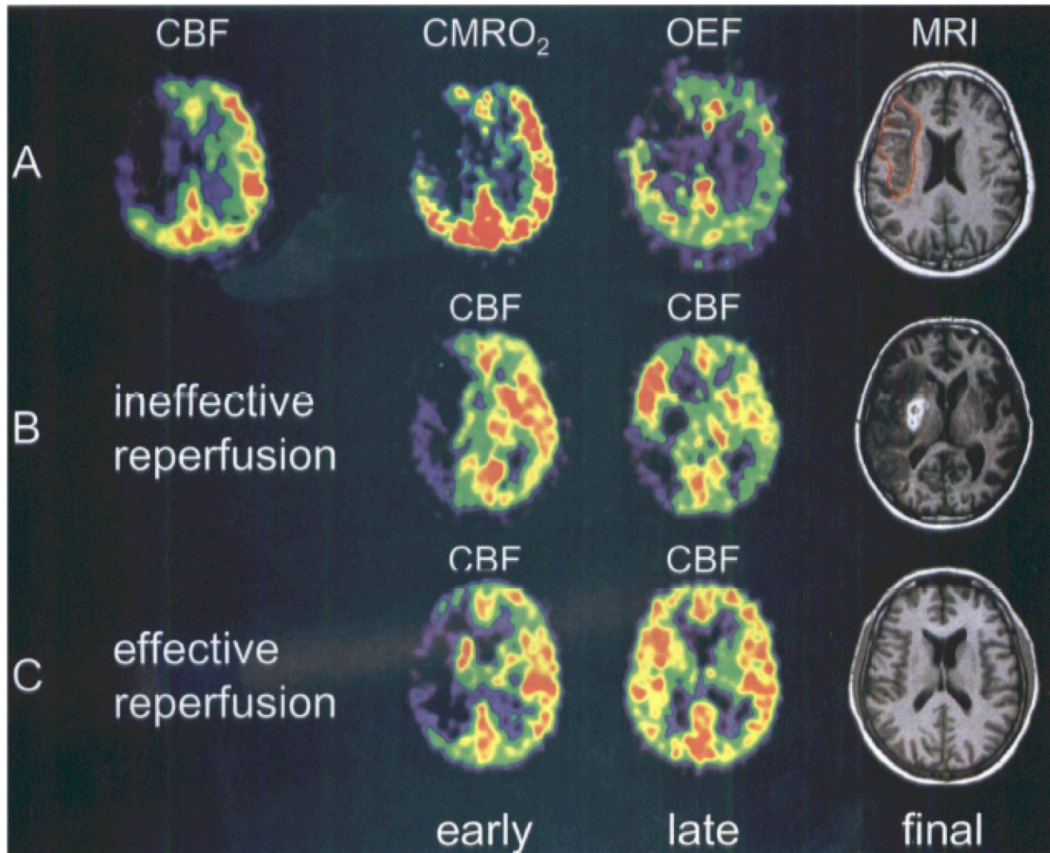


Figure 2 (from (Heiss, 2000)).

Positron emission tomography scans of a patient with ischemic stroke in the left middle cerebral artery. A) Overlying maps of cerebral blood flow, cerebral metabolic rate of oxygen, and oxygen extraction fraction predict the area of the brain that is irreversibly damaged, which is outlined in red on the magnetic resonance image. The penumbra is the area where the cerebral metabolic rate of oxygen and oxygen extraction fractions are high despite little or no cerebral blood flow. B) If too much time elapses between stroke onset and treatment, reperfusion is futile. This is clearly depicted in the final magnetic resonance image, which shows vast necrosis in the left hemisphere. C) If penumbra tissue exists when treatment begins, reperfusion is effective. In this case, the magnetic resonance image shows living tissue in the area where the stroke occurred.

a radionuclide with a reasonably long half-life of 110 minutes. If radioactively labeling erythropoietin with fluorine-18 is successful, we can then evaluate the new radiotracer's distribution in the brain.

At present, no studies have attempted to determine whether radioactively-labeled erythropoietin is an effective clinical marker of the ischemic penumbra in a stroke. If selective penumbra imaging can be accomplished, this technique may be used to identify the progress of damage after acute ischemic stroke. Establishing a novel penumbra radiotracer will enable physicians to determine whether damaged, yet viable, tissue still exists in patients, thereby arming them with knowledge of the areas that need to be targeted in subsequent therapeutic interventions. Furthermore, imaging the penumbra through the erythropoietin receptor will facilitate future studies that explore potential stroke treatments by targeting this receptor system.

1.2.2 Objectives

1.2.2.1 Radioactively Labeling Erythropoietin with Fluorine-18

Our purpose is to develop a procedure to label erythropoietin with the radionuclide fluorine-18 in order to establish [¹⁸F]-Erythropoietin with high specific activity. Since fluorine-18 is highly electron negative, it must first be introduced into a prosthetic group before attempting to label proteins. To do this, we must first synthesize a standard protein-labeling precursor, fluorine-18-labeled *N*-succinimidyl 4-[¹⁸F]fluorobenzoate ([¹⁸F]-SFB). Then, a solution of erythropoietin is added to this precursor. Afterward, the labeled protein is purified by means of high performance liquid chromatography (HPLC).

1.2.2.2 Establishing a Penumbra in the Endothelin-1 Stroke Model

Prior to testing the *in vivo* properties of [¹⁸F]-Erythropoietin, we must define the approximate size and location of the infarct, including the

penumbra, in a model of ischemic stroke. First, we evaluated the ischemic penumbra in the endothelin-1 stroke model by performing positron emission tomography scans with the established radiotracers [^{15}O]-Water and [^{18}F]-FMISO. These radiotracers reveal maps of cerebral blood flow and hypoxia, respectively. The penumbra is operationally defined as the hypoxic area or areas with little or no cerebral blood flow (Heiss, 2000).

1.2.2.3 Exploring [^{18}F]-Erythropoietin as a Penumbra Radiotracer

If the endothelin-1 stroke model has a measurable penumbra, we can then study [^{18}F]-Erythropoietin *in vivo* to see if this novel radiotracer enters the brain and binds to its selectively upregulated receptor in the penumbra. Through dynamic positron emission tomography imaging, we aim to determine the optimal post-injection peak binding time for [^{18}F]-Erythropoietin, ultimately assessing its effectiveness in revealing hypoxic, yet viable, brain tissue after a stroke.

- Chapter 2 -

Radioactively Labeling Erythropoietin with Fluorine-18

2.1 Introduction

Radioactive protein labeling is a non-specific synthesis, as proteins contain many unprotected active groups to which a radioactive labeling synthon may bind. Therefore, radiochemists have little control over the specific location where a radionuclide is incorporated into a protein's chemical structure, which could potentially alter its biological properties (Schirmacher et al., 2010). In this procedure, we first introduce the radionuclide fluorine-18 to the standard protein labeling precursor [¹⁸F]-SFB by nucleophilic substitution (Vaidyanathan and Zalutsky, 1992). This multi-step synthesis consists of radiofluorination, hydrolysis, and coupling. Afterwards, we add the protein of interest, erythropoietin, to the protein-labeling precursor and allow the reaction to proceed for a short period before purifying the final radioactively labeled protein with HPLC.

2.1.1 Erythropoietin

Erythropoietin is an endogenous, thirty-four kiloDalton glycoprotein that is neuroprotective in mammals (Arcasoy, 2008). This promising characteristic within the central nervous system makes erythropoietin a key contender in contemporary approaches to stroke treatment. When administered after a stroke, erythropoietin reduces the final infarct volume

by as much as 30% (Jerndal et al., 2010), with higher doses resulting in smaller infarcts (Minnerup et al., 2009). Initial clinical trials indicated that erythropoietin is an effective treatment for ischemic stroke in humans (Ehrenreich et al., 2002); however, subsequent trials revealed that its administration should not be combined with recombinant tissue plasminogen activator (Ehrenreich et al., 2009). A follow up study showed that the combination of these therapies not only abolishes erythropoietin's beneficial effects, but also promotes brain edema, blood-brain barrier permeability, and extracellular matrix breakdown (Zechariah et al., 2010). Clearly, much more research is needed before erythropoietin can be successfully translated to clinical use.

Both neurons and astrocytes express the erythropoietin gene (Bernaudin et al., 2000). Genes for erythropoietin and its receptor are present in the brain under normal conditions, but upon the onset of hypoxia, the typical concentrations are drastically increased (Marti et al., 1996). This is the result of a molecular signaling cascade (Brines and Cerami, 2005) that begins with hypoxia-inducible factor 1, a transcription factor that binds to the erythropoietin gene to increase its expression (Semenza et al., 1991). In turn, astrocytes produce and release erythropoietin (Juul, 2002), which then binds to its receptor on neurons (Ruscher et al., 2002). This binding initiates signaling by the protein Janus kinase 2, thereby activating phosphoinositide 3-kinase enzymes. Ultimately, these enzymes deactivate Bcl-2-associated death promoter proteins in order to reduce apoptosis resulting from hypoxia (Ruscher et al., 2002). In addition to decreasing the extent of apoptosis, erythropoietin binding inhibits calcium-induced glutamate release (Kawakami et al., 2001), which somewhat explains its neuroprotective role in stroke. Furthermore, erythropoietin reduces inflammation (Juul, 2002) and

causes cerebral vascular endothelial cells to increase their production of the vasodilator nitric oxide (Beleslin-Cokic et al., 2004), thereby allowing blood to flow through blood vessels with greater ease.

Erythropoietin exerts its neuroprotective effects through a heteroceptor complex, which is made up of both erythropoietin and common beta subunit receptors (Brines et al., 2004). Since the erythropoietin-common beta-heteroceptor is upregulated specifically in ischemic tissue (Siren et al., 2001), there is a greater concentration of this receptor in the penumbra of a stroke compared to other areas of the brain. Given this, extraneously applied erythropoietin is most likely to bind to a receptor located within this dense cluster. Therefore, by administering radioactively labeled erythropoietin to an individual who has suffered a stroke, a single positron emission tomography scan could potentially reveal the penumbra.

2.1.2 Fluorine-18

Of the radionuclides commonly used in positron emission tomography, fluorine-18 is a good option for labeling proteins. Fluorine-18 decays by 97% positron emission, so it is possible to reconstruct artifact-free positron emission tomography images. These images have exceptional spatial resolution due to the radionuclide's comparatively low energy of 649 kilo-electron volts. Moreover, fluorine-18 has a relatively long half-life of 110 minutes, which enables researchers to perform complex, time-consuming syntheses without worrying about the amount of radioactivity assimilated into the final product (Schirmacher et al., 2010). This is especially advantageous for protein labeling, as multi-step syntheses are required to incorporate fluorine-18 into organic compounds (Schirmacher et al., 2010); since fluorine-18 is the most electron negative radionuclide, it is difficult to introduce into biological molecules. For these syntheses, a labeling precursor

must first be produced and then added to a solution of the protein to be labeled.

Since non-radioactive fluorine-19 is extremely rare in nature, it is highly unlikely that a radiotracer based on fluorine-18 would be extensively contaminated with the stable fluorine-19 isotope. This way, it is possible to synthesize molecules with high specific activity, the ratio of radionuclide compared to the total amount of biological compound. This is an important feature for clinical radiopharmaceuticals for two main reasons. First, compounds with very high specific activity are less likely to cause potentially harmful side effects. Second, when interested in receptor concentrations, high specific activity indicates that more molecules are labeled with radioactive fluorine rather than non-radioactive compound (Schirmacher et al., 2010). Therefore, there is less of a chance that non-radioactive compounds occupy receptor-binding sites.

2.1.3 Predictions

Previous work shows that it is feasible to label erythropoietin with fluorine-18 (Lang and Eckelman, 1997). The protein labeling technique that uses [¹⁸F]-SFB as a precursor is well established, so this method should successfully label erythropoietin with radioactive fluorine-18.

2.2 Methods

2.2.1 Materials

Highly enriched H₂[¹⁸O] was purchased from Rotem Industries Ltd. (Arava, Israel). Ethyl 4-(trimethylammonium triflate)benzoate and non-radioactive standard were purchased from ABX (Radeberg, Germany). Erythropoietin was purchased from Creative BioMart (Shirley, New York).

All solvents, reagents, and cartridges were purchased from Sigma-Aldrich Canada Ltd. (Oakville, Ontario).

2.2.2 Synthesis of [¹⁸F]-SFB and [¹⁸F]-Erythropoietin

An IBA cyclotron (Cyclon 18/9) generated no-carrier-added [¹⁸F]F⁻ (11.1-16.6 GBq) in 2.2 mL [¹⁸O]-Water via the ¹⁸O(p,n)¹⁸F nuclear reaction with a [¹⁸O]-Water target. The [¹⁸F]F⁻ was subsequently transferred to a Scintomics Hotbox III module, where the radiosynthesis was performed. First, [¹⁸F]-SFB was synthesized using a three-step automated procedure (Tang et al., 2010). To summarize, [¹⁸F]F⁻/H₂[¹⁸O] was passed through a QMA cartridge, and ¹⁸F⁻ was eluted from the cartridge with a solution of Kryptofix_{2.2.2}[®] (10 mg, 27 μmol) and potassium carbonate (1.87 mg, 13.5 μmol) in acetonitrile/water (96:4, 1.5 mL). Next, two identical drying steps evaporated residual water by adding acetonitrile (0.5 mL) under a vacuum and stream of argon at 105°C. Afterward, the SFB precursor, ethyl 4-(trimethylammonium triflate)benzoate (5 mg) dissolved in acetonitrile (1 mL), was added to the dried [¹⁸F]F⁻/Kryptofix_{2.2.2}[®]/K⁺ complex and heated at 90°C for ten minutes. Then, tetrapropylammonium hydroxide (20 μL 1M aqueous solution in 2 mL acetonitrile) was added, and the reaction mixture was heated to 120°C for three minutes. After the acetonitrile was completely evaporated, N,N,N',N'-tetramethyl-O-(N-succinimidyl)uronium tetrafluoroborate (12 mg, 39.86 μmol) dissolved in acetonitrile (1 mL) was added, and the reaction mixture was heated to 90°C for five minutes. The solution of crude [¹⁸F]-SFB was cooled to room temperature by a stream of air and diluted with HPLC eluent (1.5 mL).

Afterward, the crude [¹⁸F]-SFB solution was injected onto an Agilent Technologies 1200 system (μBondapak C-18 column, acetonitrile/0.01M phosphoric acid, 40:60; flow 2 mL/min) equipped with a Gabi radioactivity

detector (Raytest). The radioactivity peak corresponding to the [¹⁸F]-SFB (retention time = 11 minutes) was collected in a 50 mL round bottom flask, after which the eluent was carefully evaporated *in vacuo* under gentle heating at 70°C. A solution of erythropoietin (1 mg/mL dissolved in borate buffer, pH 8-9) was then added to the [¹⁸F]-SFB and incubated at room temperature for twenty minutes. The subsequent labeled compound purification was performed on a second Agilent Technologies 1200 system equipped with a Gabi radioactivity detector (Raytest), where the mixture was passed through the HPLC system (Phenomenex Biosep-SEC-S4000, 0.1M sodium phosphate buffer pH 7.2; flow 0.7 mL/min) to obtain an injectable solution of [¹⁸F]-Erythropoietin (retention time = 15 minutes, 48-52 MBq).

2.2.3 Quality Control of [¹⁸F]-Erythropoietin

To determine whether the synthesis successfully labeled erythropoietin with fluorine-18, we compared final HPLC readouts to those of non-radioactive erythropoietin.

2.3 Quality Control Results

As demonstrated by the HPLC chromatogram (Fig. 3), erythropoietin was effectively labeled with fluorine-18. The obtained readout was identical to that of a cold standard. Upon injection, it took approximately fifteen minutes for the product to elute from the column. The first peak consisted of the fluorine-18-labeled erythropoietin, while the second peak was non-radioactive erythropoietin (retention time = 18 minutes) and the third peak contained unreacted by-products. Note that typically, the second peak's amplitude would be similar to that of the first peak; however, its amplitude appears to be off of the graph because the HPLC system was overconcentrated with product.

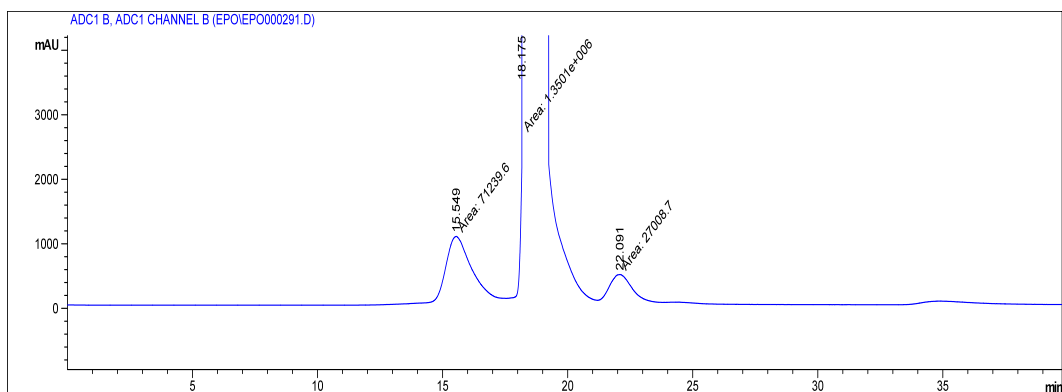


Figure 3.

Chromatogram of [^{18}F]-Erythropoietin, illustrating the purified protein peak forming at fifteen minutes.

2.4 Discussion

We found that fluorine-18 labeled erythropoietin could be obtained through the standard protein-labeling precursor [^{18}F]-SFB. This allows researchers to noninvasively study erythropoietin *in vivo*, which is particularly of interest to those attempting to develop new approaches to stroke treatment. Even though we have succeeded in radioactively labeling erythropoietin, we do not know if it will be a useful positron emission tomography radiotracer for neuroimaging, as it could possibly not cross the blood-brain barrier. Also, since we succeeded in labeling erythropoietin in our first attempt that was based on previous successful protein labeling methods, the conditions for this synthesis can be refined. Since we were able to label the protein erythropoietin with the radioactive isotope fluorine-18, we can proceed with experiments to determine its *in vivo* role in a model of ischemic stroke.

- Chapter 3 -

Establishing a Penumbra in the Endothelin-1 Stroke Model

3.1 Introduction

Before testing the properties of [^{18}F]-Erythropoietin in a living organism, it is necessary to establish a model with a reliably measurable penumbra. Of the many available *in vivo* stroke models (Sicard and Fisher, 2009), we chose to study the effects of [^{18}F]-Erythropoietin with the endothelin-1 model of focal ischemic stroke. This model was preferable to more common methods because of its ability to control for the size and location of the ischemic infarct, as well as its very low mortality rate. Once a valid penumbra model is established, further experimentation with [^{18}F]-Erythropoietin can resume.

3.1.1 Endothelin-1 Model of Focal Ischemia

Stroke rehabilitation studies regularly use the endothelin-1 stroke model, which has a very high success rate compared to the commonly used manipulation that occludes the middle cerebral artery (Chen et al., 1986). The highly invasive middle cerebral artery occlusion model was not an ideal option for this study, as it is more difficult to obtain replicable infarct sizes and locations across groups. Moreover, recovery from this surgery is variable, and a greater percentage of attempts fail to produce the intended results compared to the endothelin-1 model (Howells et al., 2010).

The endothelin-1 model allows for the exact volume and location of the infarct to be defined, which enables researchers to achieve a high degree of control over the data (Sharkey and Butcher, 1995). By maintaining consistent features such as the type, size, and location of the stroke, data from different animals can be easily compared. Moreover, endothelin-1 does not modulate the production of erythropoietin (Grenz et al., 2006), so it should not compromise the experimental outcomes of the current study. However, it is possible that this stroke model does not have either an infarct that is large enough to be measured with traditional positron emission tomography or a conventional penumbra (Fuxe et al., 1997). Therefore, it is absolutely necessary to establish the existence of a measurable stroke and penumbra in the endothelin-1 model before proceeding with additional studies using [¹⁸F]-Erythropoietin.

3.1.2 [¹⁸F]-Fluoromisonidazole

A candidate positron emission tomography radiotracer for the penumbra is fluoromisonidazole labeled with fluorine-18 (Read et al., 1998). In a clinical trial that assessed the functional outcome of hypoxic tissue in stroke patients, [¹⁸F]-FMISO binding within forty-eight hours of stroke onset was correlated with improved neurological outcome measures (Markus et al., 2004). This implies that [¹⁸F]-FMISO is trapped in a portion of hypoxic cells within the penumbra that later recover function. Moreover, positron emission tomography images of [¹⁸F]-FMISO are highly correlated between human stroke patients and animal models of stroke (Saita et al., 2004), which makes this radiotracer ideal for translational research.

Upon administration, [¹⁸F]-FMISO freely diffuses across the blood-brain barrier into living but hypoxic cells, where the low oxygen levels cause the radiotracer to accumulate by trapping its metabolites (Lee and Scott,

2007). [^{18}F]-FMISO does not reveal the infarct core because the necrotic tissue does not have the ability to metabolically trap its metabolites and the perfusion levels in the core are too low. If hypoxic cells are subsequently reperfused, any trapped [^{18}F]-FMISO is released (Takasawa et al., 2007). This characteristic is especially advantageous when imaging the ischemic penumbra, as physicians can verify whether reperfusion attempts are successful. It takes one hour for [^{18}F]-FMISO to be selectively retained within hypoxic tissue, and this remains constant for the following ninety minutes (Koh et al., 1992). Despite these advantages, this radiotracer does not distinguish between hypoxic cells that can be saved through stroke interventions and those whose oxygen levels fall below the viability threshold; thus, [^{18}F]-FMISO is an imperfect penumbra radiotracer.

3.1.3 Predictions

As a possible positron emission tomography radiotracer of the ischemic penumbra (Read et al., 1998), [^{18}F]-FMISO should clearly distinguish this area in the endothelin-1 model of stroke. Selective retention within the penumbra should occur one hour after administering [^{18}F]-FMISO. While this retention should be limited to a defined area in close proximity to where endothelin-1 is applied, healthy controls should not exhibit selective [^{18}F]-FMISO uptake.

3.2 Methods

3.2.1 Materials

Highly enriched [^{18}O]-Water was purchased from Rotem Industries Ltd. (Arava, Israel). 1-(2'-Nitro-1'-imidazolyl)-2-O-tetrahydropyranyl-3-O-toluenesulfonyl-propanediol and non-radioactive standard, as well as all solvents, reagents, and cartridges, were purchased from Sigma-Aldrich

Canada Ltd. (Oakville, Ontario). Endothelin-1 was purchased from Calbiochem (Hornby, Ontario).

3.2.2 Synthesis of [^{15}O]-Water and [^{18}F]-FMISO

An IBA cyclotron (Cyclon 18/9) generated approximately 2.2-mL no-carrier-added aqueous [^{18}F] F^- (11.1-16.6 GBq) via the $^{18}\text{O}(\text{p},\text{n})^{18}\text{F}$ nuclear reaction with a [^{18}O]-Water target, as well as oxygen-15 water via the $^{15}\text{N}(\text{p},\text{n})^{15}\text{O}$ nuclear reaction with a $^{15}\text{N}_2$ target. Once produced, the [^{18}F] F^- / H_2 [^{18}O] was transferred to a Scintomics Hotbox III module. The procedure to synthesize [^{18}F]-FMISO was slightly modified from one previously reported (Oh et al., 2005). First, [^{18}F] F^- / H_2 [^{18}O] was passed through a QMA cartridge. The $^{18}\text{F}^-$ was eluted from the cartridge with a solution of Kryptofix_{2.2.2}[®] (10 mg, 27 μmol) and potassium carbonate (1.87 mg, 13.5 μmol) in acetonitrile/water (96:4, 1.5 mL). Then, this was evaporated at 105°C under a gentle vacuum and a stream of helium. Residual water was removed by azeotropic evaporation with a second portion of acetonitrile (1.5 mL). The FMISO precursor, 1-(2'-Nitro-1'-imidazolyl)-2-O-tetrahydropyranyl-3-O-toluenesulfonyl-propanediol (5 mg, 11.8 μmol) dissolved in acetonitrile (1 mL), was added to the dried [^{18}F] F^- /Kryptofix_{2.2.2}[®]/ K^+ complex and heated at 105°C for seven minutes, then at 75°C for an additional four minutes. Following evaporation by acetonitrile, hydrochloric acid (1 mL, 1N) was added to the reaction and heated at 105°C for five minutes. Subsequently, the reaction mixture was cooled to 50°C under a stream of air, and sodium hydroxide (0.2 mL, 5N) in HPLC solvent (1.2 mL) was added to neutralize the reaction mixture.

The crude [^{18}F]-FMISO was transferred to an Agilent Technologies 1200 HPLC system (Phenomenex Luna 10 μm C-18 250 \times 10 mm column, 20 mM ammonium formate/methanol, 80:20; flow 2 mL/min) equipped with a

Gabi radioactivity detector (Raytest). The radioactivity peak (retention time = 15 minutes) was collected with a 50 mL round bottom flask. Afterwards, the eluent was carefully evaporated *in vacuo* under gentle heating, and then ethanol was added before a second evaporation step to ensure complete dryness. Lastly, the purified [¹⁸F]-FMISO was dissolved in ethanol (0.5 mL) and sodium phosphate buffer (4.5 mL, pH 7) to obtain an injectable solution of 48-52 MBq.

3.2.3 Animals

Sprague-Dawley rats (180 days old, 350-500 grams) were acquired from Charles River Laboratories International (St-Constant, Quebec). Rats were individually housed under a twelve-hour light/dark cycle with free access to food and water. Temperature consistently remained between 20-22°C. Three rats underwent surgical manipulation by means of the endothelin-1 stroke model, and three additional healthy control rats were used. See Figure 4 for a timeline of the experimental procedure. All experimentation was conducted in accordance with the guidelines of the Canadian Council on Animal Care and McGill University Animal Care Committee.

3.2.4 Surgery

Surgical manipulations were performed at the Université de Montréal. Twenty-four hours prior to surgery, enrofloxacin (5 mg/kg) was administered intramuscularly in a preventative manner. On the day of the experiment, rats were anesthetized with a gas mixture of 2% isoflurane and oxygen. Xylocaine was applied to the ears, eye ointment was applied to the eyes, and the head was positioned in a stereotaxic apparatus with non-puncturing ear bars. Body temperature was maintained at 37°C with a heating rug. A lateral incision on the skull exposed bregma, which was used

to orient the stereotaxic instrument within the dimensions of the brain atlas (Paxinos and Watson, 1997). A 0.7 millimeter round bit drill created small holes in the skull above the left motor cortex, and six injections of endothelin-1 ($0.3 \mu\text{g}/\mu\text{L}$ each) were applied via a 32 gauge Hamilton syringe at a rate of three nanoliters per second to the coordinates listed in Table 1. Each injection occurred over approximately five minutes; the entire stroke onset occurred over a period of thirty minutes. Afterwards, the holes were stopped with acrylic. Then, the skin around the wound was cleansed, sutured, and treated with Xylocaine. Post-operation, rats were monitored until reflexes were recovered and mobility was regained.

Injection	Anterior-Posterior	Medial-Lateral	Dorsal-Ventral
1	1.5	2.5	-1.5
2	1.5	3.5	-1.5
3	0.5	3.5	-1.5
4	0.5	2.5	-1.5
5	-0.5	2.5	-1.5
6	-0.5	3.5	-1.5

Table 1. Locations of endothelin-1 injections, displayed in millimeters relative to bregma (Paxinos and Watson, 1997)

3.2.5 Data Acquisition

Positron emission tomography scans were conducted at the Montreal Neurological Institute. Between two to three hours post-surgery, rats were anesthetized with isoflurane (2% concentration in oxygen) delivered through a nose cone and then placed into a micro-PET scanner (CTI Concorde R4) such that the head was situated in the center of the scanner's field of view. Throughout the duration of the scan, a healthy body temperature was maintained (37°C), and physiological parameters like heart rate and

respiration were monitored. First, a bolus injection of [^{15}O]-Water (130-204 MBq in 0.1-0.5 mL) was administered via a catheter inserted in the tail vein. A five-minute dynamic scan immediately ensued, during which data were acquired in thirty ten-second frames. Next, a ten-minute transmission scan with an external cobalt-57 photon source was obtained to later correct for attenuation within emission scans. Then, a two-hour dynamic scan revealed the extent to which [^{18}F]-FMISO (19-37 MBq in 0.1-0.5 mL) was trapped in hypoxic tissue in the brain before it was eliminated from the body. These data were collected in twelve ten-minute frames. Once the [^{18}F]-FMISO scan ended, rats were euthanized by means of anaesthetic overdose. All imaging procedures were approved by the Small Animal Imaging Laboratory at the Montreal Neurological Institute.

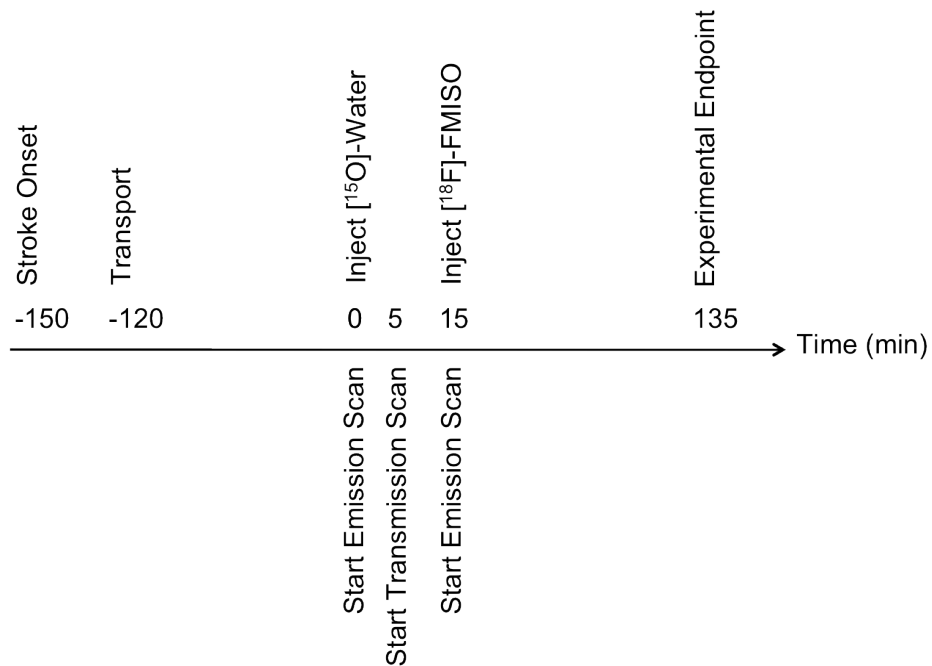


Figure 4.

Experimental time line for Objective 2.

3.2.6 Data Analysis

Sinograms were normalized and corrected for attenuation, dead time, and decay. By means of filtered back projection with a Hanning filter and cut-off frequency of 0.5 pixels per cycle, the data were reconstructed into a three-dimensional $128 \times 128 \times 63$ matrix with a voxel size of 0.06 centimeters. Images were analyzed in VINCI (Version 2.57.0, Max Planck Institute for Neurological Research, Cologne, Germany), where they were manually coregistered to a modified version of the Laboratory of Neuro Imaging magnetic resonance rat atlas (University of California Los Angeles, Los Angeles, California) using cerebral blood vessels as landmarks. For [^{15}O]-Water scans, an averaged image of the entire five-minute scan (frames 1-30) was used for later calculations; for [^{18}F]-FMISO scans, calculations were based on an averaged image of the second hour of the scan (frames 7-12). Standardized uptake values (SUV) based on body weight and radiation dose were calculated for each rat based on the following formula:

$$SUV = \text{radioactivity concentration}(t) \times \frac{\text{weight}}{\text{initial radioactivity}(t_0)}$$

An elliptical region of interest (4.5 mm^2) was delineated in the area corresponding to the motor cortex in both the left and right hemispheres and across transaxial, coronal, and sagittal planes for a total of three values within each hemisphere. Subsequent analyses were based solely on the standardized uptake values obtained in the transaxial dimension. For both experimental and controls groups, standardized uptake values were compared between the left and right hemispheres using paired t-tests ($p < .05$). Lastly, unpaired t-tests ($p < .05$) assessed standardized uptake value ratios (SUVR) between experimental and control groups, as calculated with the formula:

$$SUV \text{ ratio} = \frac{SUV_{left}}{SUV_{right}}$$

3.3 Results

3.3.1 Within-Group Comparisons

Descriptive statistics for all animals are summarized in Tables 2 and 3. Qualitative image analysis revealed that [^{18}F]-FMISO was retained within the left motor cortex in the stroke group but not in healthy controls. As expected, [^{15}O]-Water scans for the experimental group showed a lack of blood flow in the left motor cortex, and [^{18}F]-FMISO was also selectively retained in part of this region. This is visualized with the red circles in Figure 5. In controls, both [^{15}O]-Water and [^{18}F]-FMISO were evenly distributed, as shown in Figure 6. However, quantitative statistics did not reveal significant results within groups, as summarized in Table 4.

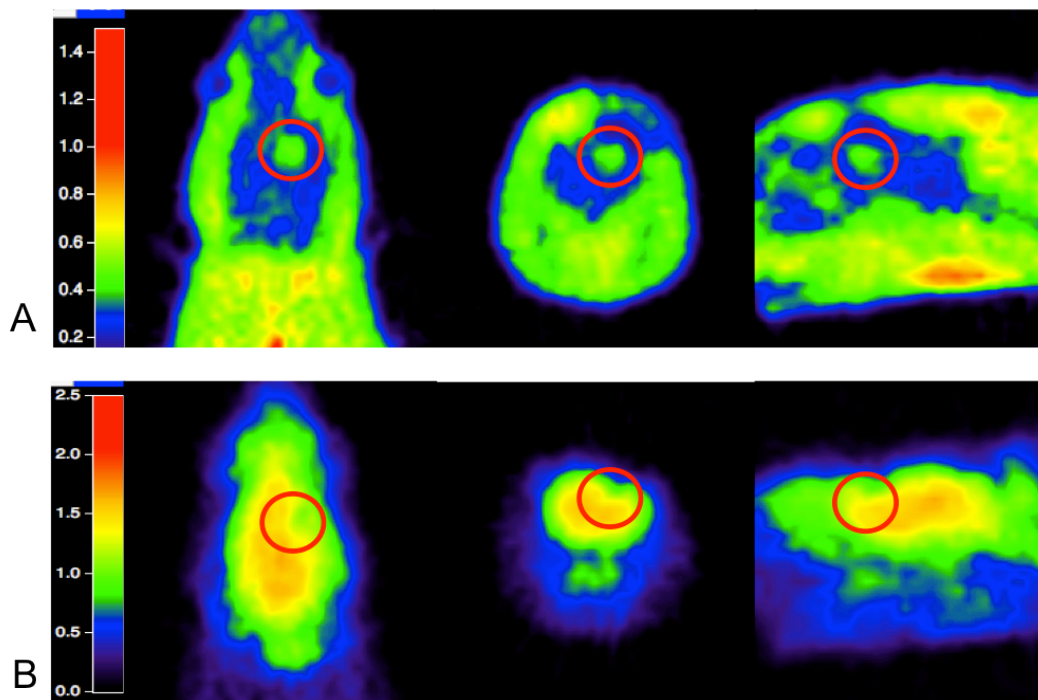


Figure 5.

Positron emission tomography standard uptake value images of Objective 2 stroke group. A) [^{18}F]-FMISO averaged over second hour of scan; B) Averaged [^{15}O]-Water scan.

Condition	n	Animal Number	Weight (g)	Injected Activity (MBq)	SUV Ratio	Transaxial		Coronal		Sagittal	
						Left	Right	Left	Right	Left	Right
						Mean (SD)					
Stroke	3	A1335	315	185.0	0.8099	1.1870 (0.1113)	1.4656 (0.0701)	1.1671 (0.2449)	1.4033 (0.1399)	1.1313 (0.2292)	1.4308 (0.1169)
		A1339	325	151.7	0.7511	1.3148 (0.1643)	1.7504 (0.1118)	1.5220 (0.2996)	1.7497 (0.2719)	1.2669 (0.3040)	1.6626 (0.3088)
		A1359	325	166.5	0.9376	17.1238 (1.6590)	18.2629 (1.4238)	15.4677 (3.7093)	17.7035 (2.6835)	15.7882 (3.7338)	17.7928 (2.2187)
Control	3	A1336	676	133.2	0.9665	1.9571 (0.1831)	2.0250 (0.1325)	1.8898 (0.2349)	1.9204 (0.1955)	1.9395 (0.1917)	1.9987 (0.1568)
		A1340	335	129.5	1.0052	2.4408 (0.1524)	2.4282 (0.1769)	2.4351 (0.1647)	2.4415 (0.2076)	2.4790 (0.1046)	2.4678 (0.1223)
		A1360	400	136.9	0.9734	1.2496 (0.0729)	1.2837 (0.0526)	1.2526 (0.1163)	1.2730 (0.0549)	1.2356 (0.0982)	1.2612 (0.0599)

Table 2. [¹⁵O]-Water descriptive statistics for Objective 2

Condition	n	Animal Number	Weight (g)	Injected Activity (MBq)	SUV Ratio	Transaxial		Coronal		Sagittal	
						Left	Right	Left	Right	Left	Right
						Mean (SD)					
Stroke	3	A1335	315	18.8	1.3638	0.4277 (0.0522)	0.3136 (0.0286)	0.4102 (0.0560)	0.3084 (0.0289)	0.4083 (0.0609)	0.3054 (0.0286)
		A1339	325	20.4	0.9565	0.7104 (0.0467)	0.7427 (0.0265)	0.7535 (0.0700)	0.7331 (0.0589)	0.6798 (0.0940)	0.7258 (0.0840)
		A1359	325	47.4	1.2096	1.1040 (0.1478)	0.9127 (0.0463)	1.0638 (0.1554)	0.8721 (0.0694)	1.0222 (0.1085)	0.8879 (0.0677)
Control	3	A1336	676	20.7	1.0058	0.8008 (0.0487)	0.7962 (0.0540)	0.7638 (0.1046)	0.7269 (0.1042)	0.7815 (0.0919)	0.7644 (0.1260)
		A1340	335	18.8	1.0526	0.6471 (0.0307)	0.6147 (0.0311)	0.6380 (0.0409)	0.6215 (0.0294)	0.6401 (0.0375)	0.6198 (0.0277)
		A1360	400	19.6	0.9648	0.7295 (0.0255)	0.7561 (0.0338)	0.7518 (0.0518)	0.7562 (0.0344)	0.7579 (0.0323)	0.7218 (0.0280)

Table 3. [¹⁸F]-FMISO descriptive statistics

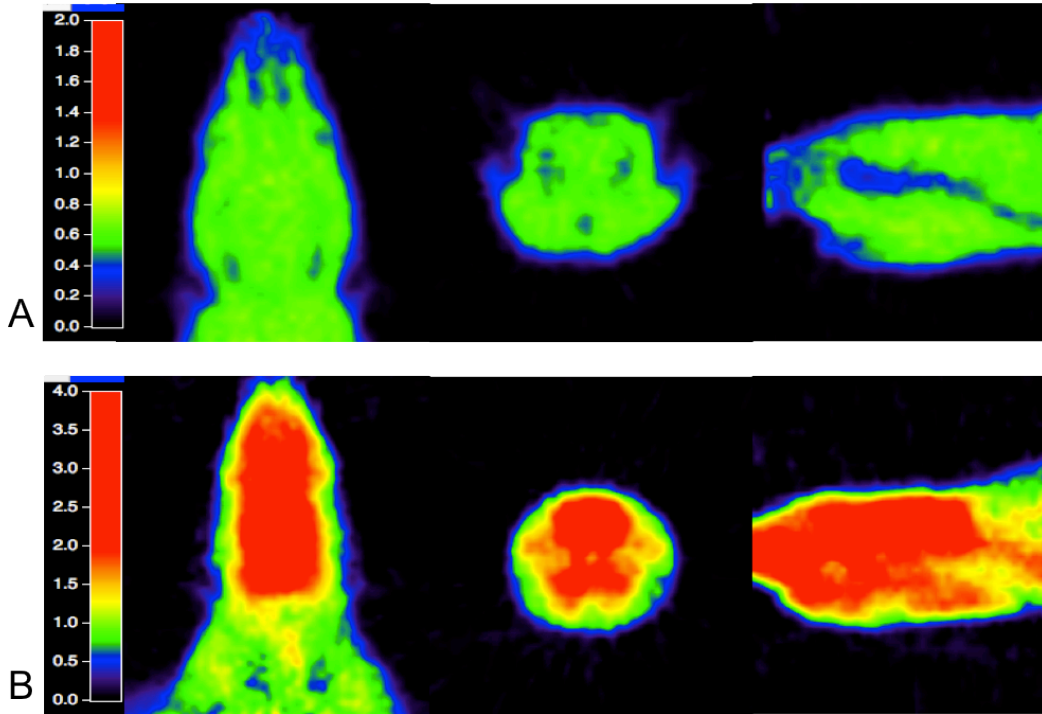


Figure 6.

Positron emission tomography standard uptake value images of Objective 2 control group. A) [^{18}F]-FMISO averaged over second hour of scan; B) Averaged [^{15}O]-Water scan.

Radiotracer	Source	df	t	p-value
[^{15}O]-Water	Stroke	2	2.335	0.1446
	Control	2	1.278	0.3295
[^{18}F]-FMISO	Stroke	2	1.388	0.2995
	Control	2	0.2031	0.8579

Table 4. Summary of paired t-tests for Objective 2

3.3.2 Between-Group Comparisons

Qualitative image analysis revealed that [^{15}O]-Water uptake was less in the left hemisphere of the experimental group compared to the right hemisphere, while there was no difference between hemispheres in controls.

Overall, there was less uptake in the experimental stroke group compared to controls, as shown in Figure 7. For [¹⁸F]-FMISO images, uptake was approximately equal in both hemispheres for controls, although there was more uptake in the left hemisphere of the experimental group (Fig. 8). Quantitative statistics did not reveal significant differences between groups, although [¹⁵O]-Water results approached significance (see Table 5).

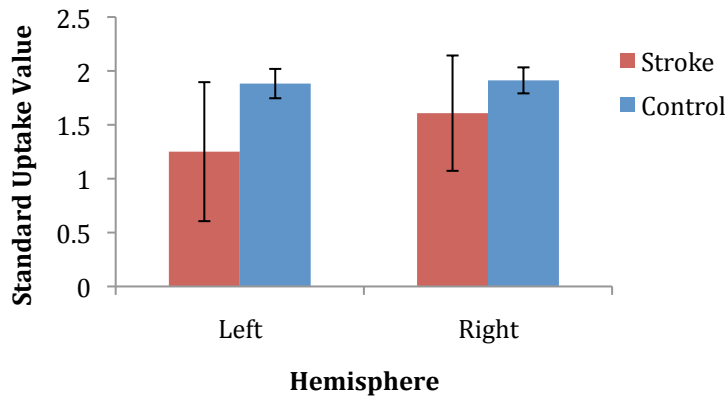


Figure 7.

Average [¹⁵O]-Water standard uptake values (\pm SD) for Objective 2, presented by experimental condition within both hemispheres.

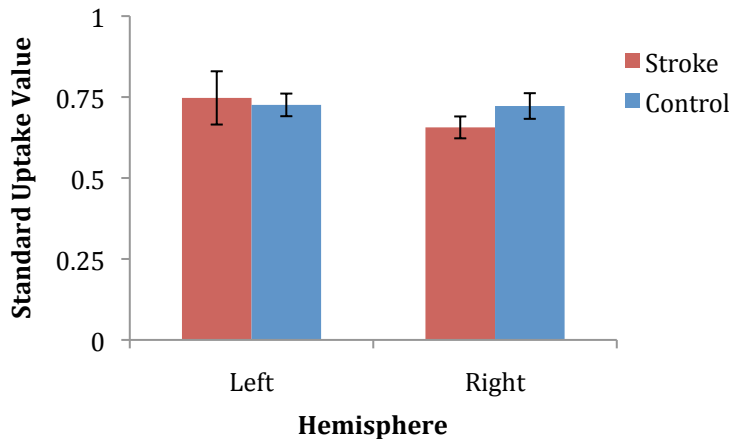


Figure 8.

Average [¹⁸F]-FMISO standard uptake values (\pm SD), presented by experimental condition within both hemispheres.

Radiotracer	df	t	p-value
[¹⁵ O]-Water	4	2.642	0.0575
[¹⁸ F]-FMISO	4	1.391	0.2366

Table 5. Summary of unpaired t-tests for Objective 2

3.3.3 Pooled Analysis of Cerebral Blood Flow Images

Since the cerebral blood flow results approached significance and were acquired with the same protocol in both experiments, we pooled these data from Objectives 2 and 3 to compare the standard uptake value ratios between the stroke and control groups. The pooled data passed both a Shapiro-Wilk normality test ($p = 0.205$) and an equal variance test ($p = 0.220$). An unpaired t-test on these data indicated that the [¹⁵O]-Water standard uptake value ratios were significantly different in the stroke group relative to the control group, $t(9) = -4.038$, $p = 0.003$. Also, the 95% confidence interval for the difference of means was $-0.300 \leq \rho \leq -0.0846$. The difference in the mean values of the two groups was greater than would be expected by chance; therefore, there is a statistically significant difference between the input groups ($p = 0.003$). A post hoc power analysis revealed that the current design was able to assess differences with a power of 94.5%.

Source	n	Missing	Mean	Standard Deviation	Standard Error of the Mean
Stroke	5	0	0.817	0.0888	0.0397
Control	6	0	1.010	0.0696	0.0284
difference = 0.193					

Table 6. Pooled [¹⁵O]-Water standard uptake value ratio descriptive statistics

3.4 Discussion

The pooled analysis of standard uptake value ratios from all [^{15}O]-Water images indicates that our model indeed induces a reliable focal ischemia at the endothelin-1 injection site. Moreover, this ischemia was large enough to be detected with [^{15}O]-Water in the rat brain during a positron emission tomography scan. This means that our endothelin-1 model, rather than the middle cerebral artery occlusion model, may be used in the future to study focal ischemia with positron emission tomography.

Within the experimental stroke group, the lack of [^{15}O]-Water uptake in the left motor cortex confirms that a stroke occurred in this region. Interestingly, overall [^{15}O]-Water uptake was less in stroke animals than in control animals. We expected cerebral blood flow in the right, i.e. normal, hemisphere of the stroke group to be about the same as that of the control group. The fact that it was not suggests that the vasoconstricting effects of endothelin-1 extended beyond the immediate area of the left motor cortex, decreasing blood flow within the entire brain. If this was the case, perhaps the entire brain experienced hypoxia to some degree, although none so much as the left motor cortex. An alternative explanation may be the concept of transcallosal diaschisis, where lesions in one cerebral hemisphere cause a reduction of blood flow in the homologous regions of the opposite hemisphere (Von Monakow, 1914). Then again, it could be that the stroke animals had a different generalized susceptibility to the effects of anesthesia compared to the control animals.

Although a positive image that may very well be the penumbra was detected with positron emission tomography imaging, we cannot conclude that the endothelin-1 model of focal stroke has a penumbra. The quantitative results were not significant, which may be due to insufficient statistical

power. Therefore, we cannot confidently conclude that this model is a valid tool to study the penumbra. Moreover, since [^{18}F]-FMISO is taken up into all hypoxic cells, we do not know whether the area identified with this radiotracer consists of tissue that falls within the functional threshold or if all tissue within this region was beyond the viability threshold. Still, there was a significant difference in cerebral blood flow in the stroke group compared to the control group. This shows that the endothelin-1 model of stroke induces a reliable ischemia that can be detected with positron emission tomography, a feature that has not previously been shown. Since the endothelin-1 model induces a reliable ischemic area, we will still examine [^{18}F]-Erythropoietin in this stroke model to see if it binds to neurons that are metabolically active.

Additionally, within the experimental group, [^{18}F]-FMISO was selectively retained in only part of the area where cerebral blood flow was absent. If [^{18}F]-FMISO is truly a penumbra marker, it should not completely overlap with the area of decreased cerebral blood flow, as part of this area, i.e. the core, would be necrotic. Conversely, the even distribution of both [^{15}O]-Water and [^{18}F]-FMISO in the control group indicated continuous blood flow and healthy tissue in the brain.

Some researchers (Strong et al., 2000, Dreier et al., 2002) believe that a true penumbra does not exist in the endothelin-1 model of stroke because this potent vasoconstrictor stops blood flow throughout a specific area. So, theoretically, this area should not be supplied with blood from collateral arteries. However, our results showed that this is not the case. Upon administering [^{18}F]-FMISO to rats that had a stroke, positron emission tomography revealed an area near the stroke's core where living, yet hypoxic, tissue was present. We do not know if this hypoxia was due to the stroke or to the surgical manipulation, so this must be determined in future studies. Still,

this finding allows researchers who use the endothelin-1 model to expand their research, knowing that the model is more comparable to ischemic stroke in humans.

- Chapter 4 -

Exploring [¹⁸F]-Erythropoietin as a Penumbra Radiotracer

4.1 Introduction

Since erythropoietin can be successfully labeled with the radionuclide fluorine-18 (see Chapter 2) and the endothelin-1 model of focal ischemia has a probable penumbra that can be measured with positron emission tomography (see Chapter 3), we can evaluate fluorine-18-labeled erythropoietin *in vivo* to see if this novel radiotracer reveals the ischemic penumbra in stroke.

4.1.1 *In Vivo* Properties of Erythropoietin

Exogenously applied erythropoietin crosses the blood-brain barrier through extracellular pathways (Banks et al., 2004). Larger molecules can cross the blood-brain barrier through one of two extracellular pathways, either between olfactory epithelial cells or through circumventricular organs (Balin et al., 1986). Since [¹⁸F]-Erythropoietin is administered intravenously in our experiment, it most likely crosses the blood-brain barrier by means of the latter option. Once in the brain, erythropoietin accumulates at 0.05-0.1% of the injected dose, peaking three hours after intravenous injection (Banks et al., 2004). Additionally, upon the onset of hypoxia, erythropoietin messenger ribonucleic acid levels in the brain peak at four hours and remain high for a full twenty-four hours (Juul, 2002). Given this, [¹⁸F]-Erythropoietin

is most likely to bind to its receptor between three to four hours after being administered, which occurs no more than three hours after stroke onset in this study.

The erythropoietin-beta common-heteroceptor complex, which is located on neurons and astrocytes (Brines et al., 2000), is upregulated in ischemic tissue in stroke (Siren et al., 2001). Furthermore, the erythropoietin receptor is expressed in both authentic and soluble forms with relatively low affinity ($K_d = 860$ pM) and approximately 10,000 binding sites per cell, and maximum specific binding occurs within four hours of administration (Yamaji et al., 1996). Recently, the existence of erythropoietin receptors on non-hematopoietic cells, such as neurons, was challenged in a study that found little to no erythropoietin receptors despite detecting its messenger ribonucleic acid (Sinclair et al., 2010). If radioactively labeled erythropoietin crosses the blood-brain barrier, its presence in targeted areas of the brain, i.e. the penumbra, should determine whether or not the erythropoietin receptor is present on neurons.

4.1.2 Predictions

We hypothesize that [^{18}F]-Erythropoietin will successfully bind to the erythropoietin-beta common-heteroceptor complex that is expressed in the ischemic penumbra, thus leading to a novel method to noninvasively image this region via positron emission tomography. Moreover, we expect the peak binding to occur within four hours after [^{18}F]-Erythropoietin is injected into the blood stream, as it will take some time for the molecule to penetrate the blood-brain barrier to enter the brain.

4.2 Methods

4.2.1 Materials

Highly enriched [^{18}O]-Water was purchased from Rotem Industries Ltd. (Arava, Israel). Ethyl 4-(trimethylammonium triflate)benzoate and non-radioactive standard were purchased from ABX (Radeberg, Germany). All solvents, reagents, and cartridges were purchased from Sigma-Aldrich Canada Ltd. (Oakville, Ontario). Erythropoietin was purchased from Creative BioMart (Shirley, New York), and endothelin-1 was purchased from Calbiochem (Hornby, Ontario).

4.2.2 Synthesis of [^{15}O]-Water and [^{18}F]-Erythropoietin

An IBA cyclotron (Cyclon 18/9) generated approximately 2.2 mL no-carrier-added aqueous [^{18}F]F $^-$ (11.1-16.6 GBq) via the $^{18}\text{O}(\text{p},\text{n})^{18}\text{F}$ nuclear reaction with a [^{18}O]-Water target and [^{15}O]-Water via the $^{15}\text{N}(\text{p},\text{n})^{15}\text{O}$ nuclear reaction with a $^{15}\text{N}_2$ target. The [^{18}F]F $^-$ /H $_2$ [^{18}O] was subsequently transferred to a Scintomics Hotbox III module, where the radiosynthesis was performed. First, [^{18}F]-SFB (1369-2146 MBq) was synthesized using a three-step automated procedure (Tang et al., 2010). Next, a solution of erythropoietin (1 mg/mL dissolved in borate buffer, pH 8-9) was added to the [^{18}F]-SFB and incubated at room temperature for twenty minutes. Afterwards, the labeled compound purification was performed on an Agilent Technologies 1200 system (Phenomenex Biosep-SEC-S4000, 0.1M sodium phosphate buffer pH 7.2; flow 0.7 mL/min) equipped with a Gabi radioactivity detector (Raytest) to obtain an injectable solution of [^{18}F]-Erythropoietin (retention time = 15 minutes, 48-52 MBq). At the end of synthesis, the radiochemical yield was 30%. Refer to Chapter 2 for a more thorough summary.

4.2.3 Animals

Sprague-Dawley rats (180 days old, 350-500 grams) were acquired from Charles River Laboratories International (St-Constant, Quebec). Rats

were individually housed under a twelve-hour light/dark cycle with free access to food and water. Temperature consistently remained between 20-22°C. Two rats underwent surgical manipulation by means of the endothelin-1 stroke model, and three additional healthy control rats were used. Refer to Figure 9 for a timeline of the experimental procedure. All experimentation was conducted in accordance with the guidelines of the Canadian Council on Animal Care and McGill University Animal Care Committee.

4.2.4 Surgery

Surgical manipulations were performed at the Université de Montréal. Briefly, rats were anesthetized with a gas mixture of 2% isoflurane and oxygen. Six injections of endothelin-1 (0.3 $\mu\text{g}/\mu\text{L}$ each) were applied to the left motor cortex. Each injection occurred over a five-minute duration, so the entire stroke onset occurred over a period of thirty minutes. Post-operation, rats were monitored until reflexes were recovered and mobility was regained. Refer to Chapter 3 for a more detailed explanation.

4.2.5 Data Acquisition

Positron emission tomography scans were conducted at the Montreal Neurological Institute. Between two to three hours post-surgery, rats were anesthetized with isoflurane (2% concentration in oxygen) delivered through a nose cone and placed into a micro-PET scanner (CTI Concorde R4) such that the head was situated in the center of the scanner's field of view. Throughout the duration of the scan, a healthy body temperature was maintained (37°C), and physiological parameters like heart rate and respiration were monitored. First, a bolus injection of [^{15}O]-Water (130-204 MBq in 0.1-0.5 mL) was administered via a catheter inserted in the tail vein. A five-minute dynamic scan immediately ensued, during which data were acquired in thirty ten-second frames. Next, a ten-minute transmission scan

with an external cobalt-57 photon source was obtained to later correct for attenuation within emission scans. Then, [¹⁸F]-Erythropoietin (19-37 MBq in 0.1-0.5 mL) was intravenously injected, and the rat was taken off of anesthesia and returned to its cage for one hour. Following this brief interlude, a three-hour dynamic scan collected [¹⁸F]-Erythropoietin data in eighteen ten-minute frames. Once this scan ended, rats were euthanized by means of anesthetic overdose. All imaging procedures were approved by the Small Animal Imaging Laboratory at the Montreal Neurological Institute.

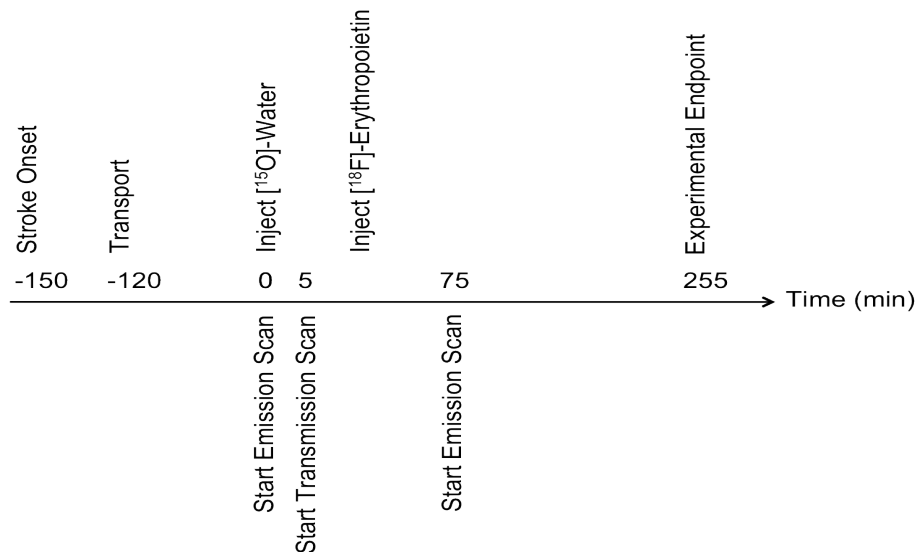


Figure 9.

Experimental time line for Objective 3.

4.2.6 Data Analysis

Sinograms were normalized and corrected for attenuation, dead time, and decay. By means of filtered back projection with a Hanning filter and cut-off frequency of 0.5 pixels per cycle, the data were reconstructed into a three-dimensional $128 \times 128 \times 63$ matrix with a voxel size of 0.06 centimeters. Images were analyzed in VINCI (Version 2.57.0, Max Planck Institute for

Neurological Research, Cologne, Germany), where they were manually coregistered to a modified version of the Laboratory of Neuro Imaging magnetic resonance rat atlas (University of California Los Angeles, Los Angeles, California) using cerebral blood vessels as landmarks. For [¹⁵O]-Water scans, an average image of the entire five-minute scan (frames 1-30) was used for later calculations. For [¹⁸F]-Erythropoietin scans, calculations were based on averaged images for each of the three scanning hours (frames 1-6, 7-12, and 13-18). Standardized uptake values based on individual body weights and radiation doses were calculated for each rat:

$$SUV = \text{radioactivity concentration}(t) \times \frac{\text{weight}}{\text{initial radioactivity}(t_0)}$$

An elliptical region of interest (4.5mm²) was delineated in the area corresponding to the motor cortex in both the left and right hemispheres and across transaxial, coronal, and sagittal planes for a total of three values within each hemisphere. Subsequent statistical analyses were based solely on the standardized uptake values obtained in the transaxial dimension. For both experimental and controls groups, standardized uptake values were compared between the left and right hemispheres using paired t-tests (ps < .05). Furthermore, unpaired t-tests (ps < .05) assessed standardized uptake value ratios between experimental and control groups, as calculated with the formula:

$$SUV \text{ ratio} = \frac{SUV_{left}}{SUV_{right}}$$

Lastly, to evaluate the radioactivity concentrations of both the [¹⁸F]-FMISO and [¹⁸F]-Erythropoietin stroke groups at the same time point, an unpaired t-test (p < .05) compared the standardized uptake value ratios for [¹⁸F]-FMISO (see Chapter 3) to those of the second scanning hour (frames 7-12) for [¹⁸F]-Erythropoietin.

Condition	n	Animal Number	Weight (g)	Injected Activity (MBq)	SUV Ratio	Transaxial		Coronal		Sagittal	
						Left	Right	Left	Right	Left	Right
						Mean (SD)					
Stroke	2	A1355	325	144.3	0.8692	1.8958 (0.1646)	2.1812 (0.0736)	1.9257 (0.3457)	2.1285 (0.1794)	1.8410 (0.3257)	2.1122 (0.1722)
		A1361	325	129.5	0.7177	0.3691 (0.0577)	0.5143 (0.0321)	0.4280 (0.0816)	0.5101 (0.0477)	0.4052 (0.0824)	0.5145 (0.0336)
Control	3	A1337	550	170.2	1.1462	1.7553 (0.0813)	1.5314 (0.1646)	1.7327 (0.1939)	1.5255 (0.2195)	1.6845 (0.2190)	1.5973 (0.1067)
		A1347	360	151.7	0.9613	1.7547 (0.1043)	1.8253 (0.0568)	1.7989 (0.1507)	1.7037 (0.2009)	1.7448 (0.1989)	1.8330 (0.1335)
		A1358	440	129.5	1.0044	3.5184 (0.2260)	3.5030 (0.2291)	3.5627 (0.2789)	3.3750 (0.3234)	3.5706 (0.1772)	3.3241 (0.2017)

Table 7. [¹⁵O]-Water descriptive statistics for Objective 3

Condition	n	Animal Number	Weight (g)	Injected Activity (MBq)	SUV Ratio	Transaxial		Coronal		Sagittal	
						Left	Right	Left	Right	Left	Right
						Mean (SD)					
Stroke	2	A1355	325	15.5	0.9832	0.2205 (0.0285)	0.2242 (0.0259)	0.2210 (0.0385)	0.2401 (0.0390)	0.2162 (0.0358)	0.2349 (0.0333)
		A1361	325	16.4	1.2793	0.1703 (0.0668)	0.1331 (0.0220)	0.1569 (0.0609)	0.1188 (0.0264)	0.1477 (0.0572)	0.1290 (0.0251)
Control	3	A1337	550	16.5	1.0411	0.2591 (0.0732)	0.2489 (0.0498)	0.2544 (0.0623)	0.2610 (0.0462)	0.2851 (0.0835)	0.2654 (0.0494)
		A1347	360	15.9	0.7992	0.1370 (0.0344)	0.1715 (0.0358)	0.1692 (0.0440)	0.1475 (0.0485)	0.1551 (0.0229)	0.1582 (0.0330)
		A1358	440	20.6	1.1089	0.3092 (0.0861)	0.2789 (0.0504)	0.3003 (0.0906)	0.2738 (0.0677)	0.3065 (0.0457)	0.2444 (0.0405)

Table 8. Descriptive statistics for [¹⁸F]-Erythropoietin (frames 1-6)

Condition	n	Animal Number	Weight (g)	Injected Activity (MBq)	SUV Ratio	Transaxial		Coronal		Sagittal	
						Left	Right	Left	Right	Left	Right
						Mean (SD)					
Stroke	2	A1355	325	15.5	0.9091	0.1986 (0.0332)	0.2184 (0.0253)	0.1936 (0.0452)	0.2109 (0.0283)	0.1864 (0.0316)	0.2093 (0.0295)
		A1361	325	16.4	1.2056	0.1794 (0.0395)	0.1489 (0.0247)	0.1583 (0.0530)	0.1391 (0.0285)	0.1550 (0.0577)	0.1335 (0.0289)
Control	3	A1337	550	16.5	1.2172	0.2276 (0.0566)	0.1870 (0.0578)	0.2407 (0.0682)	0.2097 (0.0660)	0.2835 (0.0733)	0.1912 (0.0615)
		A1347	360	15.9	0.8566	0.1346 (0.0395)	0.1571 (0.0262)	0.1668 (0.0403)	0.1447 (0.0451)	0.1206 (0.0279)	0.1437 (0.0377)
		A1358	440	20.6	1.0113	0.2782 (0.0702)	0.2751 (0.0571)	0.2677 (0.0604)	0.2725 (0.0532)	0.2767 (0.0311)	0.2574 (0.0274)

Table 9. Descriptive statistics for [¹⁸F]-Erythropoietin (frames 7-12)

Condition	n	Animal Number	Weight (g)	Injected Activity (MBq)	SUV Ratio	Transaxial		Coronal		Sagittal	
						Left	Right	Left	Right	Left	Right
						Mean (SD)					
Stroke	2	A1355	325	15.5	0.8543	0.1636 (0.0497)	0.1915 (0.0285)	0.1823 (0.0657)	0.2028 (0.0410)	0.1860 (0.0471)	0.1842 (0.0381)
		A1361	325	16.4	1.2439	0.1792 (0.0340)	0.1441 (0.0214)	0.1473 (0.0623)	0.1152 (0.0710)	0.1556 (0.0584)	0.1219 (0.0485)
Control	3	A1337	550	16.5	1.1845	0.2230 (0.0680)	0.1882 (0.0619)	0.2055 (0.0667)	0.1822 (0.0484)	0.1227 (0.0270)	0.1706 (0.0604)
		A1347	360	15.9	0.7102	0.1094 (0.0296)	0.1541 (0.0291)	0.1449 (0.0515)	0.2700 (0.0591)	0.1269 (0.0216)	0.1548 (0.0349)
		A1358	440	20.6	1.1609	0.2407 (0.0592)	0.2074 (0.0513)	0.2468 (0.0576)	0.2323 (0.0517)	0.2446 (0.0296)	0.2077 (0.0347)

Table 10. Descriptive statistics for [¹⁸F]-Erythropoietin (frames 13-18)

4.3 Results

4.3.1 Within-Group Comparisons

Descriptive statistics for all animals are summarized in Tables 6, 7, 8, and 9. Qualitative analysis of the images revealed that within the experimental group, [¹⁵O]-Water uptake was less in the left motor cortex than the rest of the brain, while this uptake was consistent throughout the brain in healthy controls. For both experimental and control groups, [¹⁸F]-Erythropoietin did not cross the blood-brain barrier, as seen in Figures 10 and 11. This result was consistent throughout the first, second, and third hours of the positron emission tomography scan. Table 10 summarizes quantitative statistics for this study, none of which were significant.

Radiotracer	Frames	Source	df	t	p-value
[¹⁵ O]-Water	1-30	Stroke	1	3.073	0.2003
		Control	2	0.6431	0.5860
[¹⁸ F]-Erythropoietin	1-6	Stroke	1	0.8163	0.5642
		Control	2	0.1069	0.9246
	7-12	Stroke	1	0.2127	0.8666
		Control	2	0.3855	0.7370
	13-18	Stroke	1	0.1146	0.9273
		Control	2	0.2978	0.7940

Table 11. Summary of paired t-tests for Objective 3

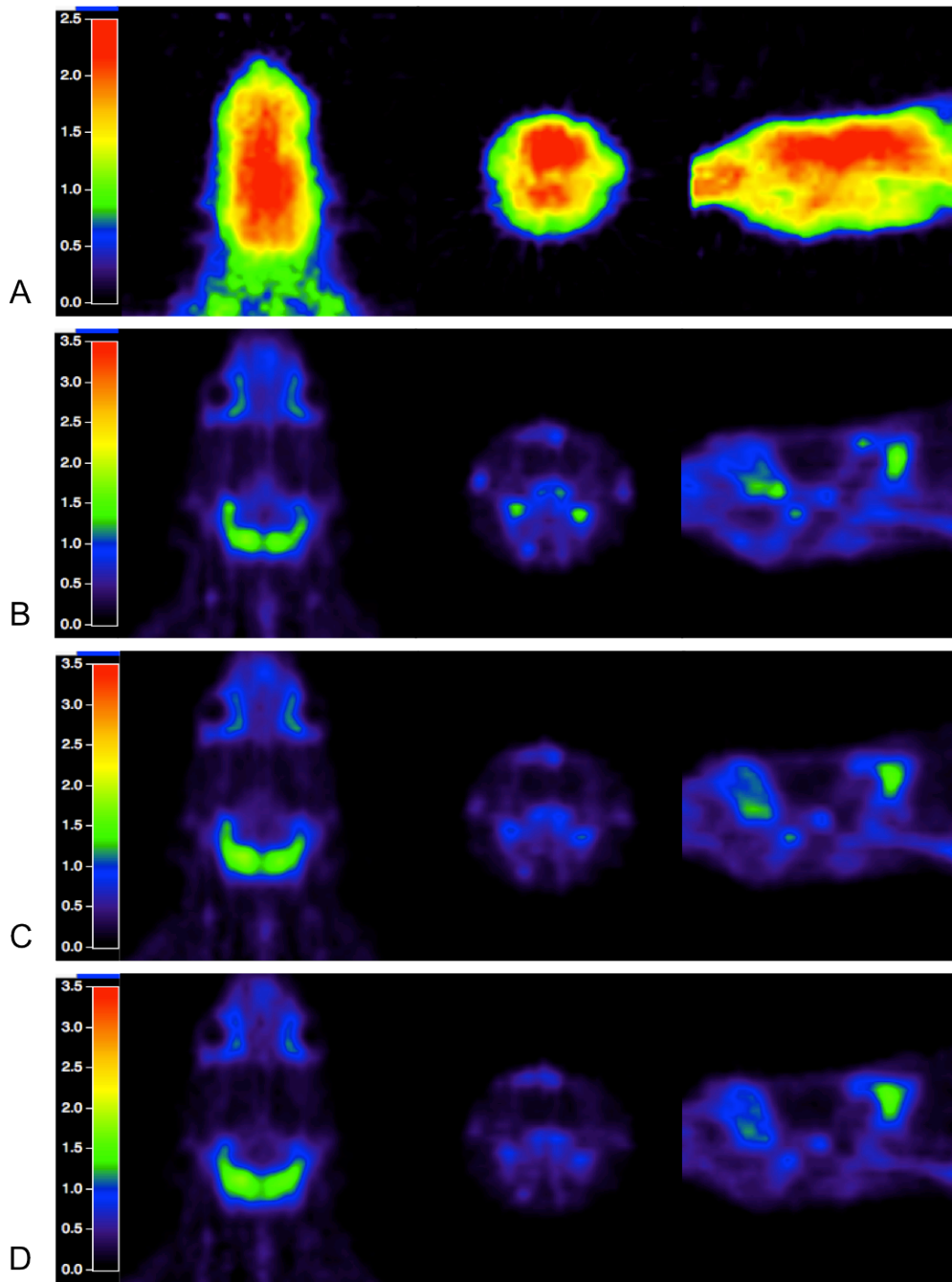


Figure 10.

Positron emission tomography standard uptake value images of $[^{18}\text{F}]$ -Erythropoietin in stroke group, shown in transaxial, coronal, and sagittal planes, respectively. A) Averaged $[^{15}\text{O}]$ -Water scan; B) $[^{18}\text{F}]$ -Erythropoietin averaged over first hour; C) $[^{18}\text{F}]$ -Erythropoietin averaged over second hour; D) $[^{18}\text{F}]$ -Erythropoietin averaged over third hour.

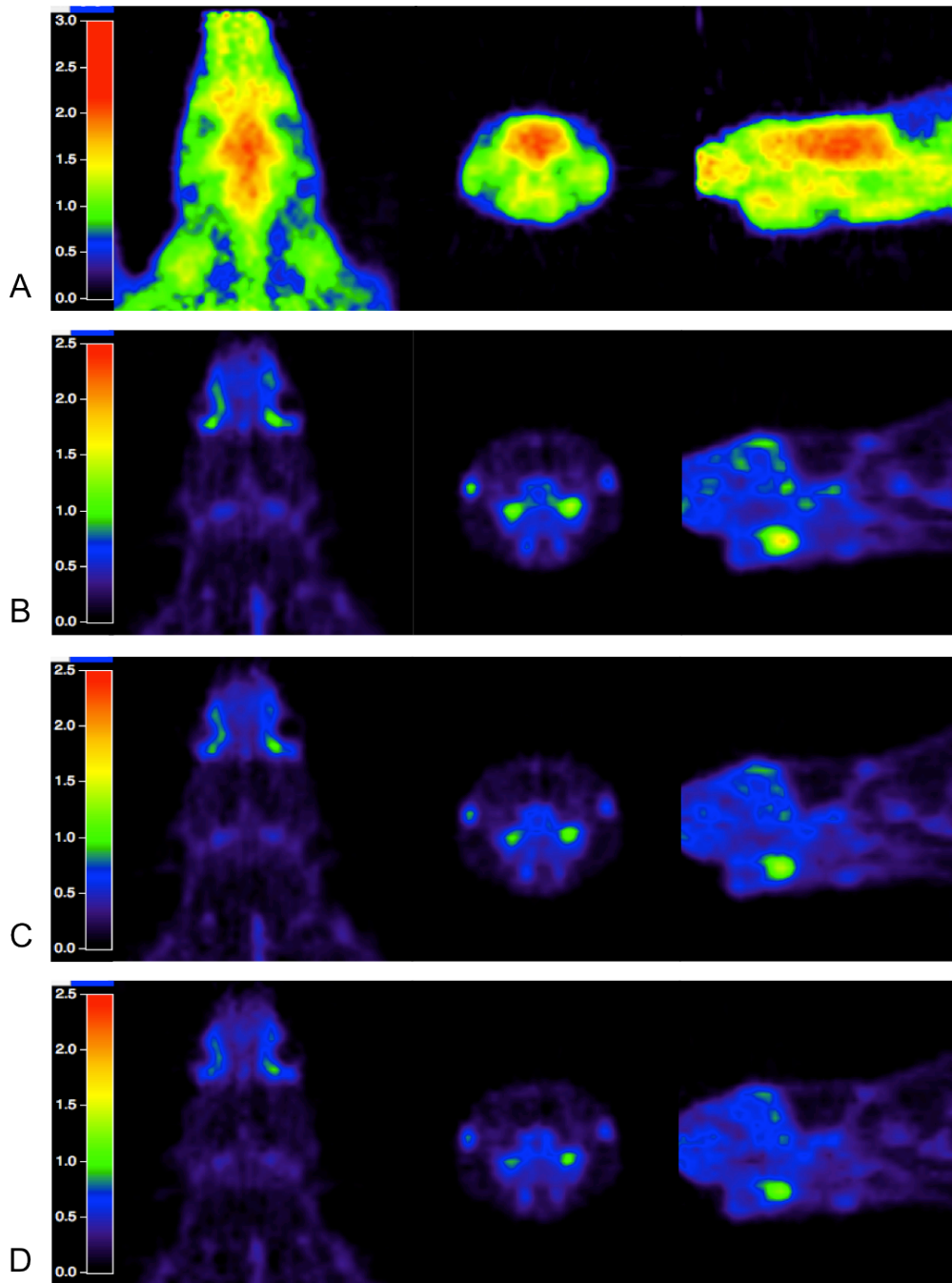


Figure 11.

Positron emission tomography standard uptake value images of [^{18}F]-Erythropoietin in control group, shown in transaxial, coronal, and sagittal planes, respectively. A) Averaged [^{15}O]-Water scan; B) [^{18}F]-Erythropoietin averaged over first hour; C) [^{18}F]-Erythropoietin averaged over second hour; D) [^{18}F]-Erythropoietin averaged over third hour.

4.3.2 Between-Group Comparisons

Qualitative image analysis revealed that overall [^{15}O]-Water uptake was less in the experimental group compared to healthy controls (Fig. 12). Also, [^{18}F]-Erythropoietin standard uptake values were low across all groups, and these further decreased over time (Fig. 13). Again, quantitative statistics did not reveal significant results between groups, as summarized in Table 11.

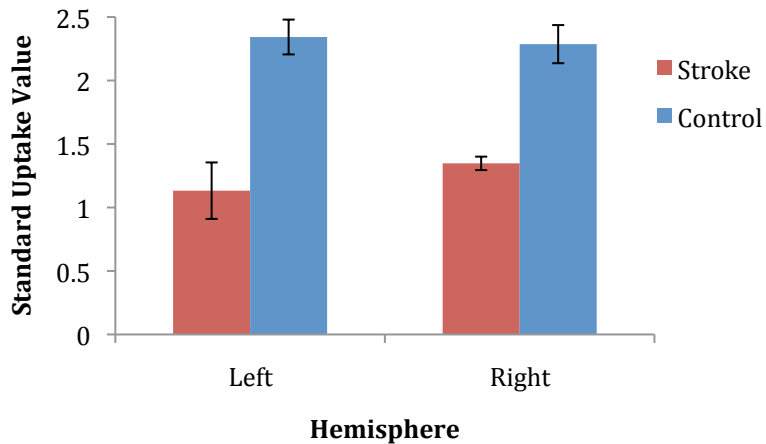


Figure 12.

Average [^{15}O]-Water standard uptake values (\pm SD) for Objective 3, presented by experimental condition within both hemispheres.

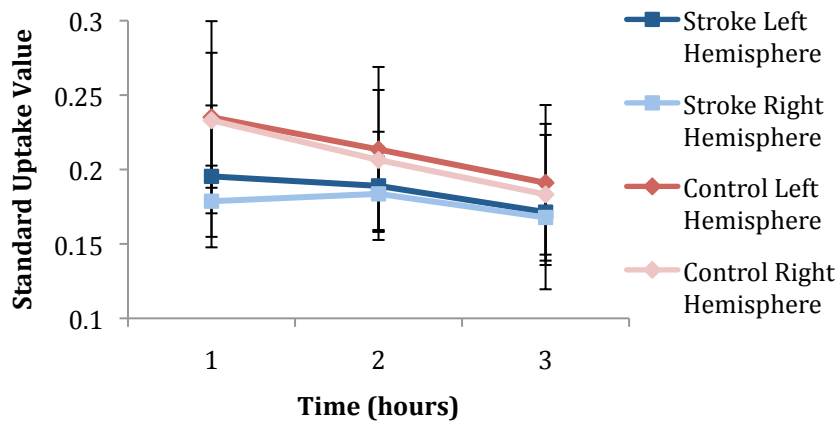


Figure 13.

Average [^{18}F]-Erythropoietin standard uptake values (\pm SD) at one, two, and three hours, presented by experimental condition within both hemispheres.

Radiotracer	Frames	df	t	p-value
[¹⁵ O]-Water	1-30	3	2.6628	0.0762
[¹⁸ F]-Erythropoietin	1-6	3	0.9039	0.4327
	7-12	3	0.1660	0.8787
	13-18	3	0.1238	0.9093

Table 12. Summary of unpaired t-tests for Objective 3

A quantitative comparison of [¹⁸F]-Erythropoietin and [¹⁸F]-FMISO images within the experimental group did not reveal significant differences, as summarized in Table 12. Qualitatively, the hypoxic area revealed in [¹⁸F]-FMISO images cannot be seen in [¹⁸F]-Erythropoietin images (Fig. 14).

Tracer	df	t	p-value
[¹⁸ F]-FMISO vs. [¹⁸ F]-Erythropoietin	3	0.6314	0.5726

Table 13. Summary of between-group comparisons for standard uptake value ratios of [¹⁸F]-FMISO and [¹⁸F]-Erythropoietin

4.4 Discussion

Positron emission tomography images revealed that [¹⁸F]-Erythropoietin did not enter the brain let alone bind to the erythropoietin receptor within the penumbra. This finding could be due to a number of possibilities, such as 1) the erythropoietin receptor is not actually upregulated in the penumbra; 2) any form of [¹⁸F]-Erythropoietin does not cross the blood-brain barrier; or 3) [¹⁸F]-Erythropoietin crosses the blood-brain barrier, just not in sufficient quantities to visualize with positron emission tomography.

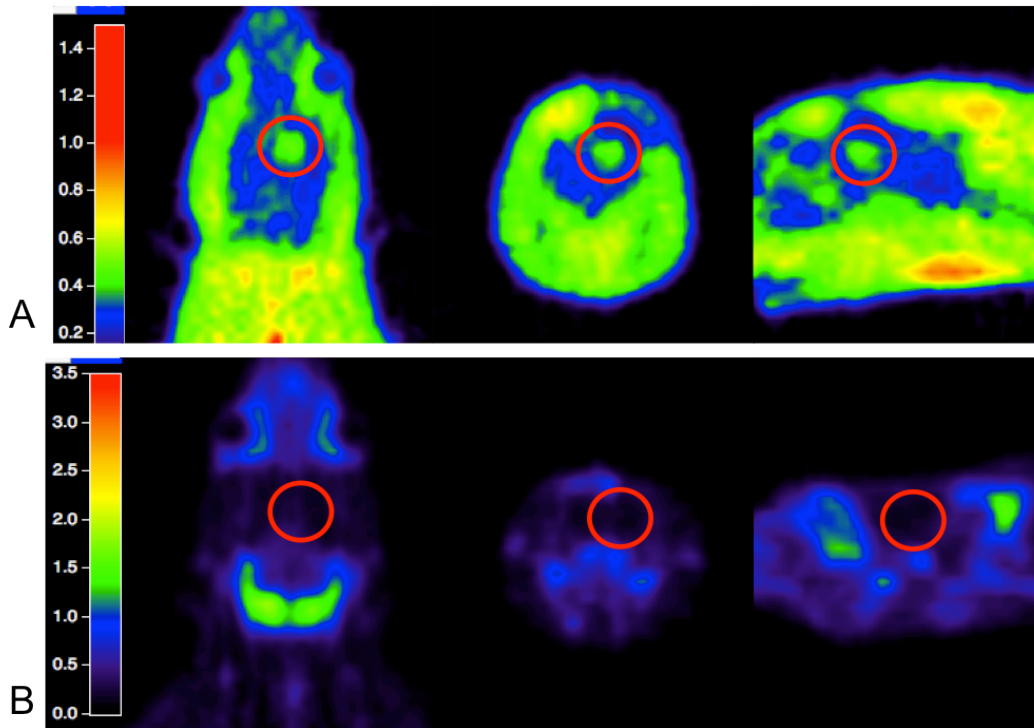


Figure 14.

Transaxial, coronal, and sagittal sections of positron emission tomography standard uptake values for A) [^{18}F]-FMISO, showing uptake in area of stroke, and B) [^{18}F]-Erythropoietin, showing no uptake in the same area.

Previous work demonstrated that the erythropoietin receptor exists in the brain (Yamaji et al., 1996); however, a recent study challenged the existence of erythropoietin receptors on non-hematopoietic cells, such as neurons (Sinclair et al., 2010). Perhaps the erythropoietin receptor does not exist on neurons, despite the presence of its messenger ribonucleic acid. Regarding the ability of [^{18}F]-Erythropoietin to cross the blood-brain barrier, the labeling position of fluorine-18 can change a biological molecule's properties (Schirmacher et al., 2010). Therefore, it is possible that radioactively labeling erythropoietin changed the protein's properties, thereby inabling it from successfully binding to its receptor in the penumbra. A different method of labeling erythropoietin could potentially alter these

findings. Additionally, it is possible that the endothelin-1 used in the stroke model somehow compromised the effects of [¹⁸F]-Erythropoietin, although Grenz et al. (2006) found that endothelin-1 does not modulate erythropoietin's production. Most likely, the radioactively labeled erythropoietin did not successfully cross the blood-brain barrier to enter the brain in sufficient quantities to be revealed with positron emission tomography.

- Chapter 5 -

General Discussion

5.1 Summary of Results

This study served as a preliminary examination of [^{18}F]-Erythropoietin as a novel positron emission tomography radiotracer for the ischemic penumbra. Although we successfully labeled erythropoietin with fluorine-18, and although we established a reliable ischemic stroke in the animal model, we were unsuccessful in establishing [^{18}F]-Erythropoietin as a novel marker of the ischemic penumbra. A penumbra-specific radiotracer could provide invaluable contributions to the current knowledge of stroke, specifically the extent to which neuroprotection plays a role in the hours following stroke onset, which has not been documented *in vivo*. Armed with this knowledge, physicians could be better equipped to treat individuals who suffer from ischemic damage, particularly regarding the timeframe in which recombinant tissue plasminogen activator can be administered. Ultimately, these results could contribute to the development of enhanced imaging techniques and clinical treatments for human stroke victims. Unfortunately, radioactively labeled erythropoietin crossed the blood-brain barrier in neither stroke models nor healthy controls; more work is necessary before this radiotracer can be properly evaluated as a penumbra marker.

5.2 Limitations

If [¹⁸F]-Erythropoietin had entered the brain to image the penumbra, it most likely would have been used to study stroke in a research capacity. Since positron emission tomography imaging is not available at every emergency room facility, [¹⁸F]-Erythropoietin could not be used as a routine method to identify the penumbra. Even if this imaging modality was available, it takes lots of time and manual resources to synthesize radiotracers and operate scanners. Moreover, erythropoietin would have to be on demand at every location that accommodates positron emission tomography. Since time is of essence in stroke treatment, these limitations would make it somewhat challenging to use [¹⁸F]-Erythropoietin as a diagnostic tool.

A major confound within this study is the lack of a sham surgery comparison group. Within the experimental group, stroke was induced via stereotaxic surgery. Consequently, we cannot confidently conclude that [¹⁸F]-FMISO images were due to hypoxia from stroke, as this could be due to the surgical manipulation. Further experimentation should include a sham surgery comparison group instead of healthy controls in order to eliminate confounding variables associated with stereotaxic surgery. Comparing the experimental stroke group to a sham surgery group would effectively enable us to conclude that the hypoxic area revealed by the [¹⁸F]-FMISO scan actually resulted from a stroke.

5.3 Future Directions

Future studies could develop ways to label this protein with a different radionuclide, like iodine-124 or gallium-68, to see if this would work better. In addition to potentially modifying the *in vivo* properties of erythropoietin, this method would also allow for longer scanning sessions using positron

emission tomography. This way, researchers could evaluate the *in vivo* effects of [¹⁸F]-Erythropoietin within a greater interval to see if it enters the brain outside of the time frame captured with the current study.

Also, modifying the conditions for the [¹⁸F]-Erythropoietin synthesis could change its *in vivo* properties, thereby enabling [¹⁸F]-Erythropoietin to enter the brain. Another option consists of attaching erythropoietin to a transport molecule that enables it to cross the blood-brain barrier with greater ease. For instance, Zhang et al. (2010) found that erythropoietin attached to a protein transduction domain more readily crosses the blood-brain barrier while retaining its neuroprotective properties. Regardless of the methodology used, there are still several options for how to increase erythropoietin's ability to cross the blood-brain barrier.

In addition, radioactively labeling erythropoietin derivatives, like carbamylated erythropoietin, could result in successful positron emission tomography imaging of the penumbra. Like erythropoietin, its derivatives are also neuroprotective in stroke (Villa et al., 2007), and in some cases, these derivatives provide more protection than erythropoietin (Brines et al., 2004). These compounds have different biological properties than erythropoietin, so they could be better equipped at crossing the blood-brain barrier to bind to the erythropoietin receptor in the penumbra. Unfortunately, we could not explore our research question using a derivative of erythropoietin. These compounds are highly controlled by the pharmaceutical industry, which makes them all but unattainable for research purposes. Still, they are the best alternatives to erythropoietin.

5.4 Conclusions

Developing novel radiotracers, specifically to image processes within the brain, requires considerable time and resources. It is not sufficient to just

successfully radioactively label these molecules, as new radiotracers must cross the blood-brain barrier within a relatively short period of time in order to be of use to neurologists. Erythropoietin remains a viable candidate for a penumbra radiopharmaceutical; however, more work is needed in order to optimize its utility for neuroimaging.

References

- Arcasoy MO (2008) The non-haematopoietic biological effects of erythropoietin. *Br J Haematol* 141:14-31.
- Astrup J, Siesjo BK, Symon L (1981) Thresholds in cerebral ischemia - the ischemic penumbra. *Stroke* 12:723-725.
- Balin BJ, Broadwell RD, Salzman M, el-Kalliny M (1986) Avenues for entry of peripherally administered protein to the central nervous system in mouse, rat, and squirrel monkey. *J Comp Neurol* 251:260-280.
- Banks WA, Jumbe NL, Farrell CL, Niehoff ML, Heatherington AC (2004) Passage of erythropoietic agents across the blood-brain barrier: a comparison of human and murine erythropoietin and the analog darbepoetin alfa. *Eur J Pharmacol* 505:93-101.
- Baron JC (2001) Perfusion thresholds in human cerebral ischemia: historical perspective and therapeutic implications. *Cerebrovasc Dis* 11 Suppl 1:2-8.
- Baron JC, von Kummer R, del Zoppo GJ (1995) Treatment of acute ischemic stroke. Challenging the concept of a rigid and universal time window. *Stroke* 26:2219-2221.
- Beleslin-Cokic BB, Cokic VP, Yu X, Weksler BB, Schechter AN, Noguchi CT (2004) Erythropoietin and hypoxia stimulate erythropoietin receptor and nitric oxide production by endothelial cells. *Blood* 104:2073-2080.
- Bernaudin M, Bellail A, Marti HH, Yvon A, Vivien D, Duchatelle I, Mackenzie ET, Petit E (2000) Neurons and astrocytes express EPO mRNA: oxygen-sensing mechanisms that involve the redox-state of the brain. *Glia* 30:271-278.

- Brines M, Cerami A (2005) Emerging biological roles for erythropoietin in the nervous system. *Nat Rev Neurosci* 6:484-494.
- Brines M, Grasso G, Fiordaliso F, Sfacteria A, Ghezzi P, Fratelli M, Latini R, Xie QW, Smart J, Su-Rick CJ, Pobre E, Diaz D, Gomez D, Hand C, Coleman T, Cerami A (2004) Erythropoietin mediates tissue protection through an erythropoietin and common beta-subunit heteroreceptor. *Proc Natl Acad Sci U S A* 101:14907-14912.
- Brines ML, Ghezzi P, Keenan S, Agnello D, de Lanerolle NC, Cerami C, Itri LM, Cerami A (2000) Erythropoietin crosses the blood-brain barrier to protect against experimental brain injury. *Proc Natl Acad Sci U S A* 97:10526-10531.
- Center IS (2012) *Ischemic Stroke*. vol. 2012.
- Chen ST, Hsu CY, Hogan EL, Maricq H, Balentine JD (1986) A model of focal ischemic stroke in the rat: reproducible extensive cortical infarction. *Stroke* 17:738-743.
- Dani KA, Thomas RG, Chappell FM, Shuler K, MacLeod MJ, Muir KW, Wardlaw JM (2011) Computed tomography and magnetic resonance perfusion imaging in ischemic stroke: definitions and thresholds. *Ann Neurol* 70:384-401.
- Dreier JP, Kleeberg J, Petzold G, Priller J, Windmuller O, Orzechowski HD, Lindauer U, Heinemann U, Einhaupl KM, Dirnagl U (2002) Endothelin-1 potently induces Leao's cortical spreading depression in vivo in the rat: a model for an endothelial trigger of migrainous aura? *Brain* 125:102-112.
- Ehrenreich H, Hasselblatt M, Dembowski C, Cepek L, Lewczuk P, Stiefel M, Rustenbeck HH, Breiter N, Jacob S, Knerlich F, Bohn M, Poser W, Ruther E, Kochen M, Gefeller O, Gleiter C, Wessel TC, De Ryck M,

- Itri L, Prange H, Cerami A, Brines M, Siren AL (2002) Erythropoietin therapy for acute stroke is both safe and beneficial. *Mol Med* 8:495-505.
- Ehrenreich H, Weissenborn K, Prange H, Schneider D, Weimar C, Wartenberg K, Schellinger PD, Bohn M, Becker H, Wegrzyn M, Jahnig P, Herrmann M, Knauth M, Bahr M, Heide W, Wagner A, Schwab S, Reichmann H, Schwendemann G, Dengler R, Kastrup A, Bartels C (2009) Recombinant human erythropoietin in the treatment of acute ischemic stroke. *Stroke* 40:e647-656.
- Furlan M, Marchal G, Viader F, Derlon JM, Baron JC (1996) Spontaneous neurological recovery after stroke and the fate of the ischemic penumbra. *Ann Neurol* 40:216-226.
- Fuxe K, Bjelke B, Andbjør B, Grahn H, Rimondini R, Agnati LF (1997) Endothelin-1 induced lesions of the frontoparietal cortex of the rat. A possible model of focal cortical ischemia. *Neuroreport* 8:2623-2629.
- Grenz A, Klein J, Kohle C, Freudenthaler S, Proksch B, Wu J, Wolf S, Osswald H, Gleiter CH (2006) Effect of endothelin-1 on erythropoietin production in a rat model under normoxia and functional carbon monoxide-induced hypoxia. *Naunyn Schmiedeberg's Arch Pharmacol* 373:342-348.
- Heiss WD (2000) Ischemic penumbra: evidence from functional imaging in man. *J Cereb Blood Flow Metab* 20:1276-1293.
- Heiss WD (2011) The ischemic penumbra: correlates in imaging and implications for treatment of ischemic stroke. The Johann Jacob Wepfer award 2011. *Cerebrovasc Dis* 32:307-320.
- Heiss WD, Sobesky J, Smekal U, Kracht LW, Lehnhardt FG, Thiel A, Jacobs AH, Lackner K (2004) Probability of cortical infarction predicted by

flumazenil binding and diffusion-weighted imaging signal intensity: a comparative positron emission tomography/magnetic resonance imaging study in early ischemic stroke. *Stroke* 35:1892-1898.

Hinkle JL, Guanci MM (2007) Acute ischemic stroke review. *J Neurosci Nurs* 39:285-293, 310.

Howells DW, Porritt MJ, Rewell SS, O'Collins V, Sena ES, van der Worp HB, Traystman RJ, Macleod MR (2010) Different strokes for different folks: the rich diversity of animal models of focal cerebral ischemia. *J Cereb Blood Flow Metab* 30:1412-1431.

Ito H, Kanno I, Kato C, Sasaki T, Ishii K, Ouchi Y, Iida A, Okazawa H, Hayashida K, Tsuyuguchi N, Kuwabara Y, Senda M (2004) Database of normal human cerebral blood flow, cerebral blood volume, cerebral oxygen extraction fraction and cerebral metabolic rate of oxygen measured by positron emission tomography with ¹⁵O-labelled carbon dioxide or water, carbon monoxide and oxygen: a multicentre study in Japan. *Eur J Nucl Med Mol Imaging* 31:635-643.

Jerndal M, Forsberg K, Sena ES, Macleod MR, O'Collins VE, Linden T, Nilsson M, Howells DW (2010) A systematic review and meta-analysis of erythropoietin in experimental stroke. *J Cereb Blood Flow Metab* 30:961-968.

Juul S (2002) Erythropoietin in the central nervous system, and its use to prevent hypoxic-ischemic brain damage. *Acta Paediatr Suppl* 91:36-42.

Kawakami M, Sekiguchi M, Sato K, Kozaki S, Takahashi M (2001) Erythropoietin receptor-mediated inhibition of exocytotic glutamate release confers neuroprotection during chemical ischemia. *J Biol Chem* 276:39469-39475.

- Koh WJ, Rasey JS, Evans ML, Grierson JR, Lewellen TK, Graham MM, Krohn KA, Griffin TW (1992) Imaging of hypoxia in human tumors with [F-18]fluoromisonidazole. *Int J Radiat Oncol Biol Phys* 22:199-212.
- Lang L, Eckelman WC (1997) Labeling proteins at high specific activity using N-succinimidyl 4-[18F](fluoromethyl) benzoate. *Appl Radiat Isot* 48:169-173.
- Latchaw RE, Alberts MJ, Lev MH, Connors JJ, Harbaugh RE, Higashida RT, Hobson R, Kidwell CS, Koroshetz WJ, Mathews V, Villablanca P, Warach S, Walters B (2009) Recommendations for imaging of acute ischemic stroke: a scientific statement from the American Heart Association. *Stroke* 40:3646-3678.
- Lee ST, Scott AM (2007) Hypoxia positron emission tomography imaging with 18f-fluoromisonidazole. *Semin Nucl Med* 37:451-461.
- Markus R, Donnan G, Kazui S, Read S, Reutens D (2004) Penumbra topography in human stroke: methodology and validation of the 'Penumbrogram'. *Neuroimage* 21:1252-1259.
- Marti HH, Wenger RH, Rivas LA, Straumann U, Digicaylioglu M, Henn V, Yonekawa Y, Bauer C, Gassmann M (1996) Erythropoietin gene expression in human, monkey and murine brain. *Eur J Neurosci* 8:666-676.

- Minnerup J, Heidrich J, Rogalewski A, Schabitz WR, Wellmann J (2009)
The efficacy of erythropoietin and its analogues in animal stroke
models: a meta-analysis. *Stroke* 40:3113-3120.
- Muir KW, Buchan A, von Kummer R, Rother J, Baron JC (2006) Imaging
of acute stroke. *Lancet Neurol* 5:755-768.
- Oh SJ, Chi DY, Mosdzianowski C, Kim JY, Gil HS, Kang SH, Ryu JS,
Moon DH (2005) Fully automated synthesis of
[18F]fluoromisonidazole using a conventional [18F]FDG module.
Nucl Med Biol 32:899-905.
- Paxinos G, Watson C (1997) *The Rat Brain in Stereotaxic Coordinates*. San
Diego: Academic Press.
- Read SJ, Hirano T, Abbott DF, Sachinidis JI, Tochon-Danguy HJ, Chan JG,
Egan GF, Scott AM, Bladin CF, McKay WJ, Donnan GA (1998)
Identifying hypoxic tissue after acute ischemic stroke using PET and
18F-fluoromisonidazole. *Neurology* 51:1617-1621.
- Roger VL, Go AS, Lloyd-Jones DM, Benjamin EJ, Berry JD, Borden WB,
Bravata DM, Dai S, Ford ES, Fox CS, Fullerton HJ, Gillespie C,
Hailpern SM, Heit JA, Howard VJ, Kissela BM, Kittner SJ,
Lackland DT, Lichtman JH, Lisabeth LD, Makuc DM, Marcus GM,
Marelli A, Matchar DB, Moy CS, Mozaffarian D, Mussolino ME,
Nichol G, Paynter NP, Soliman EZ, Sorlie PD, Sotoodehnia N,
Turan TN, Virani SS, Wong ND, Woo D, Turner MB (2012) Heart

disease and stroke statistics--2012 update: a report from the American Heart Association. *Circulation* 125:e2-e220.

Ruscher K, Freyer D, Karsch M, Isaev N, Megow D, Sawitzki B, Priller J, Dirnagl U, Meisel A (2002) Erythropoietin is a paracrine mediator of ischemic tolerance in the brain: evidence from an in vitro model. *J Neurosci* 22:10291-10301.

Saita K, Chen M, Spratt NJ, Porritt MJ, Liberatore GT, Read SJ, Levi CR, Donnan GA, Ackermann U, Tochon-Danguy HJ, Sachinidis JI, Howells DW (2004) Imaging the ischemic penumbra with ¹⁸F-fluoromisonidazole in a rat model of ischemic stroke. *Stroke* 35:975-980.

Schirmacher R, Wangler C, Schirmacher E (2010) Fluorine-18 Radiochemistry: Theory and Practice. In: *Pharmaceutical Radiochemistry*, vol. 1 (Wester, H. J., ed), pp 5-74 Furstenfeldbruck: Scintomics.

Semenza GL, Neifelt MK, Chi SM, Antonarakis SE (1991) Hypoxia-inducible nuclear factors bind to an enhancer element located 3' to the human erythropoietin gene. *Proc Natl Acad Sci U S A* 88:5680-5684.

Sharkey J, Butcher SP (1995) Characterisation of an experimental model of stroke produced by intracerebral microinjection of endothelin-1

adjacent to the rat middle cerebral artery. *J Neurosci Methods* 60:125-131.

Sicard KM, Fisher M (2009) Animal models of focal brain ischemia. *Exp Transl Stroke Med* 1:7.

Sinclair AM, Coxon A, McCaffery I, Kaufman S, Paweletz K, Liu L, Busse L, Swift S, Elliott S, Begley CG (2010) Functional erythropoietin receptor is undetectable in endothelial, cardiac, neuronal, and renal cells. *Blood* 115:4264-4272.

Siren AL, Knerlich F, Poser W, Gleiter CH, Bruck W, Ehrenreich H (2001) Erythropoietin and erythropoietin receptor in human ischemic/hypoxic brain. *Acta Neuropathol* 101:271-276.

Sobesky J, Zaro Weber O, Lehnhardt FG, Hesselmann V, Neveling M, Jacobs A, Heiss WD (2005) Does the mismatch match the penumbra? Magnetic resonance imaging and positron emission tomography in early ischemic stroke. *Stroke* 36:980-985.

Strong AJ, Smith SE, Whittington DJ, Meldrum BS, Parsons AA, Krupinski J, Hunter AJ, Patel S, Robertson C (2000) Factors influencing the frequency of fluorescence transients as markers of peri-infarct depolarizations in focal cerebral ischemia. *Stroke* 31:214-222.

Suwanwela N, Koroshetz WJ (2007) Acute ischemic stroke: overview of recent therapeutic developments. *Annu Rev Med* 58:89-106.

- Taber KH, Black KJ, Hurley RA (2005) Blood flow imaging of the brain: 50 years experience. *J Neuropsychiatry Clin Neurosci* 17:441-446.
- Takasawa M, Beech JS, Fryer TD, Hong YT, Hughes JL, Igase K, Jones PS, Smith R, Aigbirhio FI, Menon DK, Clark JC, Baron JC (2007) Imaging of brain hypoxia in permanent and temporary middle cerebral artery occlusion in the rat using 18F-fluoromisonidazole and positron emission tomography: a pilot study. *J Cereb Blood Flow Metab* 27:679-689.
- Tang G, Tang X, Wang X (2010) A facile automated synthesis of N-succinimidyl 4-[18F]fluorobenzoate ([18F]SFB) for 18F-labeled cell-penetrating peptide as PET tracer. *Journal of Labelled Compounds and Radiopharmaceuticals* 53:543-547.
- Vaidyanathan G, Zalutsky MR (1992) Labeling proteins with fluorine-18 using N-succinimidyl 4-[18F]fluorobenzoate. *Int J Rad Appl Instrum B* 19:275-281.
- van der Kooij MA, Groenendaal F, Kavelaars A, Heijnen CJ, van Bel F (2008) Neuroprotective properties and mechanisms of erythropoietin in in vitro and in vivo experimental models for hypoxia/ischemia. *Brain Res Rev* 59:22-33.
- Villa P, van Beek J, Larsen AK, Gerwien J, Christensen S, Cerami A, Brines M, Leist M, Ghezzi P, Torup L (2007) Reduced functional deficits, neuroinflammation, and secondary tissue damage after

treatment of stroke by nonerythropoietic erythropoietin derivatives. *J Cereb Blood Flow Metab* 27:552-563.

Von Monakow C (1914) Diaschisis. In: *Brain and behaviour I: Moods, states and mind*(Pribam, K. H., ed), pp 27-36 Baltimore: Penguin.

Wahl RL, Buchanan JW (2002) *Principles and Practice of Positron Emission Tomography*: Lippincott Williams & Wilkins.

Wang X, Pang Y, Ku G, Xie X, Stoica G, Wang LV (2003) Noninvasive laser-induced photoacoustic tomography for structural and functional in vivo imaging of the brain. *Nat Biotechnol* 21:803-806.

Yamaji R, Okada T, Moriya M, Naito M, Tsuruo T, Miyatake K, Nakano Y (1996) Brain capillary endothelial cells express two forms of erythropoietin receptor mRNA. *Eur J Biochem* 239:494-500.

Zechariah A, Elali A, Hermann DM (2010) Combination of tissue-plasminogen activator with erythropoietin induces blood-brain barrier permeability, extracellular matrix disaggregation, and DNA fragmentation after focal cerebral ischemia in mice. *Stroke* 41:1008-1012.